Journal of Ethnopharmacology 338 (2025) 119074

Contents lists available at ScienceDirect

Journal of Ethnopharmacology

journal homepage: www.elsevier.com/locate/jethpharm

Identification of anti-inflammatory and anti-cancer compounds targeting the NF-κB-NLRP3 inflammasome pathway from a phytochemical library of the *Sideritis* genus

Rümeysa Yücer [a], Angela Schröder [b], Gülaçtı Topçu [c,d], Thomas Efferth [a,*]

[a] Department of Pharmaceutical Biology, Institute of Pharmaceutical and Biomedical Sciences, Johannes Gutenberg University, Staudinger Weg 5, 55128, Mainz, Germany
[b] Theophrastus Paracelsus Foundation, 64367, Mühltal, Germany
[c] Department of Pharmacognosy and Phytochemistry, Faculty of Pharmacy, Bezmialem Vakif University, 34093, Fatih, Istanbul, Turkiye
[d] Drug Application & Research Center (DARC), Bezmialem Vakif University, 34093, Fatih, Istanbul, Turkiye

ARTICLE INFO

Keywords:
Inflammasome
Molecular docking
Lamiaceae
Microscale thermophoresis
Verbascoside
Virtual drug screening

ABSTRACT

Ethnobotanical relevance: For centuries, the aerial parts of *Sideritis* species have been known for their medicinal properties as herbal teas. Although the antioxidant and anti-inflammatory properties of the genus have been widely documented, the underlying mechanisms are yet to be sufficiently clarified.
Aim of the study: We investigated the anti-inflammatory and anticancer activities of phytochemicals of the *Sideritis* genus.
Material and methods: Through literature mining, a chemical library containing 657 components of the *Sideritis* genus was formed. We studied these compounds for binding to NLRP3 and NF-κB proteins *in silico* by virtual drug screening and molecular docking, and *in vitro* by microscale thermophoresis (MST). Liquid chromatography-high-resolution mass spectrometry analysis (LC-HRMS) was performed in the *Sideritis* extracts. One of the identified compounds, verbascoside, was investigated for its cytotoxic activity by mining a panel of 49 tumor cell lines in the data repository of the National Cancer Institute (NCI, USA).
Results: Virtual screening and molecular docking results highlighted two compounds targeting both proteins of interest, *i.e.*, verbascoside (acteoside) and apigenin 7,4′-bis(trans-*p*-coumarate), as both had lowest binding energies of less than −10 kcal/mol. Using MST, we then verified that both compounds bound to the target proteins. Verbascoside bound to NLRP3 and NF-κB with K_d values of 0.67 ± 0.18 μM and 0.01 ± 0.08 μM, while apigenin 7,4′-bis(trans-*p*-coumarate) had K_d values of 4.60 ± 1.66 μM and 0.27 ± 0.75 μM, respectively. Verbascoside was abundant in the *Sideritis* extracts, according to LC-HRMS analysis. Since inflammation is strongly related to carcinogenesis, we investigated the anticancer activity of verbascoside in the second part of this study. We investigated the activity of verbascoside in 49 tumor cell lines of the NCI. Comparing its activity with 81 standard anticancer drugs revealed numerous interactions with DNA-damaging agents (alkylators, topoisomerase I/II inhibitors, antimetabolites), indicating that verbascoside may also affect the DNA of tumor cells. We further investigated the involvement of verbascoside in several main drug resistance mechanisms, *i.e.*, ABC transporters, oncogenes, tumor suppressors, cellular proliferation rates, and other parameters. Except for the correlation to the mutational status of NRAS, no other significant relationships were found, indicating that verbascoside is not involved in most of the common drug resistance mechanisms. Two-dimensional cluster analysis-based heatmap generation of a proteomic profile from 40 out of 3171 proteins revealed a significant correlation between the expression of these proteins in 49 tumor cell lines, and the cellular response to verbascoside. This indicates that the presence of these proteins is a determinant for sensitivity or resistance to this natural product.
Conclusion: The database established here represents a valuable resource for the screening of bioactivites of the *Sideritis* genus. The experimental validation of the anti-inflammatory and cytotoxic activities of selected compounds proved that virtual drug screening and molecular docking are suitable tools for the identification of putative drug candidates. Verbascoside was among the top 10 compounds binding to two key anti-inflammatory

* Corresponding author.
E-mail addresses: ryuecer@students.uni-mainz.de (R. Yücer), angela.schroeder@zuv.uni-heidelberg.de (A. Schröder), gtopcu@bezmialem.edu.tr (G. Topçu), efferth@uni-mainz.de (T. Efferth).

https://doi.org/10.1016/j.jep.2024.119074
Received 6 March 2024; Received in revised form 9 October 2024; Accepted 8 November 2024
Available online 9 November 2024

proteins, NLRP3 and NF-kB. Additionally, data from the NCI indicate that verbascoside is not linked to main drug resistance mechanisms.

Abbreviations

ABC	ATP-binding cassette
BuOH	butanol
COVID-19	coronavirus disease 2019
DCM	dichloromethane
DPPH	2,2-diphenyl-1-picrylhydrazyl
EGFR	epidermal growth factor receptor
EMA	European Medicines Agency
EtOAc	ethyl acetate
GC	gas chromatography
GSTP1	glutathione S-transferase P1
HSP90	heat shock protein 90
IL	interleukin
L	liter
LBE	lowest binding energy
LC-MS	liquid chromatography – mass spectrometry
LC-HRMS	liquid chromatography-high-resolution mass spectrometry
LPS	lipopolysaccharide
LRR	leucine-rich repeat domain
MST	microscale thermophoresis
NACHT	nucleotide-binding oligomerization domain, leucine-rich repeat and pyrin domain containing 1
NCI-DTP	Developmental Therapeutics Program, National Cancer Institute, USA
NF-κB	nuclear factor kappa B cells
NLRP3	nucleotide-binding oligomerization domain, leucine rich repeat and pyrin domain containing 3
NMR	nuclear magnetic resonance
NRAS	Neuroblastoma RAS viral oncogene homolog
pKi	predicted inhibition constant
PYD	N-terminal pyrin domain SARS-CoV2, severe acute respiratory syndrome coronavirus type 2
TNF-α	tumor necrosis factor alpha
TP53	tumor suppressor 53 kD.1

1. Introduction

The *Sideritis* genus is a member of the Lamiaceae family and is mainly found throughout Mediterranean countries, but also appears in Central Europe and Near East. It is represented by more than 150 species worldwide and is utilized in traditional medicine as an herbal tea or flavoring agent. Infusions are consumed for colds, coughs, wound healing, and antiulcerogenic and gastrointestinal complaints (Akcos et al., 1999; Aneva et al., 2019; Baytop, 1999; Gunbatan et al., 2020).

The monograph of the European Medicines Agency (EMA) also asserts its usage as a traditional herbal product to relieve mild gastrointestinal disorders and coughs associated with colds (HPMC, 2015). Extracts of different *Sideritis* species and isolated compounds from this genus have been shown to possess anti-inflammatory (De Las Heras et al., 1999; Hernández-Pérez and Rabanal Gallego, 2002; Küpeli et al., 2007; Tadic et al., 2012), antioxidant (Armata et al., 2008; Ertas et al., 2009; Gonzalez-Burgos et al., 2016; Tunalier et al., 2004), antiviral (Bruno et al., 2002; Kilic et al., 2020), anti-ulcerogenic (Aboutabl et al., 2002; Alcaraz and Tordera, 1988; Gürbüz et al., 2005), and antimicrobial activities (Dulger et al., 2005; Loğoğlu et al., 2006; Rodriguez-Linde et al., 1994), as well as neuroprotective (González-Burgos et al., 2013; Heiner et al., 2018; Knörle, 2012) and anticancer effects (Jeremic et al., 2013; Tasheva et al., 2023).

Like many other plants, the secondary metabolites of the *Sideritis* genus comprise terpenes (Çarıkçı et al., 2023; Kılıç et al., 2003; Piozzi et al., 2006; Topcu et al., 2011), phenolic compounds (including flavonoids) and their glycosides (Halfon et al., 2013; Petreska et al., 2011), phenylpropanoid glycosides (Ezer et al., 1992; Kirmizibekmez et al., 2012), lignans (Fraga et al., 1995; Kırmızıbekmez et al., 2021), iridoids (Hanoğlu et al., 2020; Venditti et al., 2016), as well as sterols and aliphatic structures (Aboutabl et al., 2002; Fraga et al., 2009) which are responsible for their biological activities.

Previously published literature mainly focuses on phytochemical contents, extraction methods, and the activity of extracts and isolated phytochemicals of this genus, however, there is only scarce information on the cellular and molecular mechanisms of action (Aneva et al., 2019). Since the pharmacological activities of *Sideritis* plants are mostly attributed to their antioxidant and anti-inflammatory effects, we focused on the underlying mechanisms. For this reason, we have chosen the inflammasome pathway for further investigation.

Inflammasomes are multiprotein complexes within the cells and represent key components of the immune system, playing an important role in a wide range of diseases, including cancer (Moossavi et al., 2018), viral infections (*e.g.*, COVID-19) (Islamuddin et al., 2022; Zhao and Zhao, 2020), vector-borne diseases (*e.g.*, borreliosis) (Oosting et al., 2016), cardiovascular diseases (*e.g.*, atherosclerosis (Baldrighi et al., 2017; van der Heijden et al., 2017), atrial fibrillation (Qiu et al., 2018; Yao et al., 2018) cardiomyopathy (Bracey et al., 2013; Suetomi et al., 2018)), neurodegenerative diseases (*e.g.*, multiple sclerosis (Cui et al., 2022; Govindarajan et al., 2020), Alzheimer's disease (Flores et al., 2022; Sharma et al., 2022), Parkinson's disease (Cheng et al., 2020; Pike et al., 2022)), type-2 diabetes (Gora et al., 2021), and gout (Lin et al., 2021; Szekanecz et al., 2019). NLRP3, the most studied and well-known inflammasome, is composed of three different components, *i.e.*, LRR (leucine-rich repeat domain), NACHT (nucleotide-binding oligomerization domain, leucine-rich repeat and pyrin domain containing 1), and PYD (N-terminal pyrin domain). Upon stimulation, PYD interacts with the pyrin domain of adapter proteins (ASC). Afterward, the CARD domain of ASC interacts with the CARD domain of procaspase-1, forming the NLRP3 inflammasome. The inflammasome assembly causes the release of active caspase-1, which converts proinflammatory cytokines (pro-IL-1β and pro-IL-18) to their active forms (IL-1β and IL-18). It also cleaves gasdermin-D, a protein required for inflammation-induced cell death (pyroptosis) (Swanson et al., 2019). Preclinical as well as clinical evidence implicates that aberrant NLRP3 inflammasome activation plays an important role in a wide range of major diseases, including cancer. NLRP3 exerted pro-tumor activity in several cancer types. Increased secretion of IL-1β and IL-18 through NLRP3 dysregulation in the tumor microenvironment led to tumor progression by promoting angiogenesis, immunosuppression and metastasis (Tengesdal et al., 2023). The inflammasome also has a crucial function in causing vast inflammatory processes seen in severe and fatal cases of COVID-19. Active inflammasome molecules were observed in lung tissue and peripheral blood mononuclear cells of patients with fatal cases of COVID-19 (Rodrigues et al., 2021; Toldo et al., 2021). SARS-CoV-2 induces NLRP3 inflammasome assembly, leading to the release of IL-1β, IL-18, and IL-6, in A549 lung cells and THP-1

macrophages (Chittasupho et al., 2023; Dissook et al., 2023; Semmarath et al., 2022). The NLRP3 inflammasome formation was activated by the SARS-COV-2 nucleocapsid protein N (Pan et al., 2021), spike protein (Kucia et al., 2021), envelope protein E (Yalcinkaya et al., 2021), and ORF3a-encoded viroprotein (Xu et al., 2022). All in all, NLRP3 is becoming an increasingly viable drug target for mitigating disease progression in a wide range of illnesses. NLRP3 expression is closely linked to NF-κB activation (He et al., 2016; Kinoshita et al., 2015), and NF-κB is crucial for NLRP3 expression. Inhibition of NF-κB leads to the suppression of NLRP3 expression, highlighting the significance of targeting NF-κB in our study (Boaru et al., 2015). Similar to NLRP3, NF-κB has a crucial role in cancer development and progression, excessive activation of its signaling pathways has been shown in a variety of tumor tissues, and studies on this pathway for targeted cancer therapy have gained popularity (Xia et al., 2018). We aimed to investigate the mechanisms of *Sideritis* phytochemicals involved in the NLRP3 inflammasome pathway. For this reason, a chemical library was generated containing all known compounds of this genus. To the best of our knowledge, this is the first comprising phytochemical *Sideritis* library worldwide contains 657 compounds. PyRx-based *in silico* drug screening using a phytochemical *Sideritis* library, and NLRP-3 and NF-κB as target proteins were conducted. Then, molecular docking with the selected top compounds using AutoDock was performed. Selected commercially available phytochemicals with the lowest binding energies (LBE) *in silico* were used for microscale thermophoresis experiments to verify the binding of the compounds to the target proteins *in vitro*. LC-HRMS study showed the abundance of the verbascoside. The transcriptome and proteome expression data, as well as the correlation between the $\log_{10}IC_{50}$ values of 49 verbascoside-treated tumor cell lines, and those treated with 81 conventional anticancer drugs, have been deposited at the NCI's Developmental Therapeutics Program.

2. Materials and methods

2.1. Construction of a phytochemical sideritis library

Beginning with review articles (Fraga, 2012; González-Burgos et al., 2011; Gonzalez et al., 1979; Piozzi et al., 2006), all publications of the Web of Science database covering phytochemical research on *Sideritis* species were systematically mined. The search was conducted with the search term ''*Sideritis*''. These compounds were isolated and structurally elucidated by NMR techniques, detected by liquid chromatography – mass spectrometry (LC-MS) techniques, and by gas chromatography (GC) techniques from the aerial parts of the plant. Compounds detected to be less than 1% in GC analyses were not included. Collected compounds were categorized by their structure types. For *in silico* assays, about two thirds of the compounds and the positive controls (MCC950 and Hu-211) were downloaded as 3-dimensional (3D) structures in "sdf" file format from the PubChem database (pubchem.ncbi.nlm.nih.gov). All other substances which were not included in this database were first manually drawn as 2D structures using ChemDraw (revvitysignals.com/products/research/chemdraw) and then converted to 3D structures with energy minimization. All compounds were converted to "pdb" files using Chem3D (revvitysignals.com/products/research/chemdraw), and then converted to "pdbqt" files using PyRx (sourceforge.net/projects/pyrx). "Sdf" files were directly converted to "pdb" files by OpenBabel (sourceforge.net/projects/openbabel) and then converted to "pdbqt" files by PyRx.

2.2. Virtual screening with PyRx

NLRP3 (PDB ID: 6npy) and NF-κB (PDB ID: 1a3q) proteins were obtained from the RCSB Protein Data Bank (rcsb.org). For NLRP3, chain B, which is protein kinase R, serine/threonine-protein kinase Nek7, was removed and for NF-κB, nucleic acids and replicate chains were taken out. Hetero-atoms and water molecules were deleted, polar hydrogen atoms were added, missing atoms were repaired, Kollman charges were added, and finally saved in "pdbqt" format on AutoDockTools 1.5.6 (https://ccsb.scripps.edu/mgltools/).

The library compounds and the known NLRP3 inhibitor MCC950, as positive control (Coll et al., 2019), were virtually screened using PyRx towards NLRP3 within the area where ADP binds to the NACHT domain (dimensions x, y, z: 52, 52, 50; centers for x, y, z: 79.595, 96.502, 94.028; spacing: 0.5). For NF-κB, the active site was determined by the CASTp server, the grip parameters were set (dimensions x, y, z: 54, 54, 54; centers for x, y, z: 29.358, 79.653, −25.026; spacing: 0.5), and screened using PyRx. The known NF-κB inhibitor dexanabiol (HU-211) (Jüttler et al., 2004) served as positive control. The lowest binding affinities (kcal/mol) of the compounds were calculated and ranked.

2.3. Molecular docking with AutoDock 4.2.6

Out of 657 compounds subjected to PyRx-based virtual screening, the top 120 were selected and subjected to molecular docking with AutoDock 4.2.6 together with the positive controls, to predict their interactions with the active protein sites mentioned above. For each ligand, all "gpf", "glg", and "dpf" files and maps were created. The Lamarckian algorithm was applied with 250 runs and 2,500,000 energy evaluations. Molecular docking was conducted using the supercomputer MOGON and advisory services offered by Johannes Gutenberg University Mainz (hpc.uni-mainz.de), which is a member of the AHRP (Alliance for High-Performance Computing in Rhineland-Palatinate, ahrp.info).

2.4. Liquid chromatography-high-resolution mass spectrometry (LC-HRMS) analysis

2.4.1. Plant material and extract preparation

Sideritis stricta was obtained from Konya (Türkiye) in 2017. Herbarium samples were obtained from Selçuk University, Medicinal and Endemic Plants Training and Research Farm and are kept in Selçuk University Medical and Endemic Plants Herbarium. Locality Information: Medicinal and Endemic Plants Training and Research Farm, Selçuk University, 2019, 1020 m, YK 1043 (SÜTEB 61). Botanical identification was performed by Prof. Dr. Yuksel Kan. A dry sample (1 kg) from the fine ground of the aerial parts of *S. stricta* was extracted with methanol (10 L) overnight by maceration. The solutions were filtered with filter papers (Whatman paper) and evaporated with a rotary evaporator (Heidolph 94200, Bioblock Scientific). Highly viscose methanol extracts were dissolved in water:methanol (10:1) solvent and subjected to liquid-liquid extraction with petrol etherium (PE, 4 × 800 ml), dichloromethane (DCM, 4 × 500 ml), ethyl acetate (EtOAc, 3 × 500 ml), and butanol (BuOH, 3 × 500 ml) (Merck, Germany) successively. Solvents were evaporated later yielding PE (24.8 g), DCM (5.5 g), EtOAc (9.8 g), and BuOH (135.3 g) extracts.

2.4.2. Instruments and chromatographic conditions of LC-HRMS

Liquid chromatography-high resolution mass spectrometry (LC-HRMS) was used to determine the phenolic content of four extracts of *Sideritis stricta*. The technique had been previously developed, validated, and mentioned (Kızıltaş et al., 2021). The mass parameters and qualifications of the target compounds were also studied and shown earlier (Bingol et al., 2021; Özer et al., 2020). The method's LC and mass conditions are described in depth in the supporting documentation (Tables S1 and S2, and Figs. S1–S3).

2.5. Microscale thermophoresis

The confirmation of the *in silico* binding results was performed with selected compounds using microscale thermophoresis (MST). Recombinant NLRP3 (Origene, TP750176) and NF-κB p100/p52 (Abcam, ab125611) were labeled with the Monolith Protein Labeling Kit RED-NHS 2nd Generation (Cat. No. M0-L011, NanoTemper Technologies,

Munich, Germany). Sixteen different concentrations of the compounds ranging from 400 μM to 12.2 nM were prepared with a constant DMSO ratio of 2% in MST buffer (50 mM Tris-Base, 150 mM NaCl, 10 mM $MgCl_2$ and 0.05% v/v Tween 20, completed to 100 mL with H_2O dest.). The concentration of labeled NLRP3 and NF-κB proteins was measured by Nanodrop 1000 (PEQLAB, Erlangen, Germany) (c = 3475 nM and 1650 nM, respectively). The labeled proteins were added as 1:1 dilutions, thus reducing the concentration of the compounds by half. The three chosen compounds, verbascoside, isoverbascoside, and apigenin-7-,4′-bis-(trans-*p*-coumarate) were obtained from Fischer Analytics GmbH (Bingen am Rhein, Germany).

The samples were measured by utilizing Monolith NT.115 (Nano Temper Technologies, Munich, Germany). The MST power was set to 10%, 20%, 40%, 60%, and 80%, and the light emitting diodes (LED) power was 35% and 40% for NLRP3 and NF-κB, respectively, at 20 °C. The fitting curves with K_d values were calculated with MO.Affinity analysis software (NanoTemper Technologies).

2.6. Tumor cell lines

Drug-sensitive wild-type CCRF-CEM and their multidrug-resistant, P-glycoprotein (ABCB1) overexpressing subline, CEM/ADR5000 were obtained from Prof. Axel Sauerbrey (/University of Jena, Jena, Germany. The cell culture conditions as well as the description of doxorubicin resistance and the cross-resistance profile of CEM/ADR5000 cells were reported (Kimmig et al., 1990; Efferth et al., 2008).

A wide panel of 81 human tumor cell lines from the NCI's Developmental Therapeutics Program (NCI-DTP), (Bethesda, MD, USA) was used (https://dtp.cancer.gov; accessed on February 27, 2024) to gain insights into verbascoside's possible mode of action (Alley et al., 1988). The correlation of the $\log_{10}IC_{50}$ values of 49 cell lines treated with verbascoside and those treated with 81 standard anticancer compounds, as well as the transcriptomic and proteomic expression data were deposited in the NCI-DTP database. The cell lines were derived from leukemia, melanoma, non-small cell lung cancer, colon cancer, renal cancer, ovarian cancer, breast cancer, prostate cancer, and tumors of the central nervous system. Because of this variety, we were able to evaluate the efficacy and potential mechanisms of verbascoside in many cancer types, giving us a broad understanding of its anticancer qualities.

2.7. Cluster analyses of proteomic expression data

The mass-spectrometry-based proteomic expression profiles of the NCI tumor cell line panel (https://dtp.cancer.gov) (Guo et al., 2015) were subjected to the Pearson correlation test aiming to establish correlations between the expression data of different genes implicated in anticancer drug resistance (*ABCB1, ABCB5, ABCC1, ABCG2, EGFR*, mutated *TP53* and *NRAS, HSP90,* and *GSTP1*) and the $\log_{10}IC_{50}$ values of the NCI cell line panel for verbascoside. The test calculated significance values and rank correlation coefficients as a relative measure for the linear dependence of two variables. Based on their correlation coefficients (*r*-values), each of the top 20 proteins directly or inversely correlating with the $\log_{10}IC_{50}$ values for verbascoside was selected. For validation, we utilized positive controls exhibiting a strong correlation with their respective resistance mechanisms (epirubicin for *ABCB1,* maytansine for *ABCB5,* vinblastine for *ABCC1*, pancratistatin for *ABCG2*, erlotinib for *EGFR,* 5-fluorouracil for mutated TP53 and for cellular proliferation, doxorubicin for mutated *NRAS* and for *GSTP1*, geldanamycin for *HSP90*). These 40 proteins were subjected to hierarchical cluster analysis (Ward method) to construct a two-dimensional heatmap using the CIMMiner software (https://discover.nci.nih.gov/cimminer/) based on agglomerative clustering. The chi-square ($\chi 2$) test was used within the Excel program to validate the frequency distributions for pairs of observed and expected variables, identifying dependencies derived from cluster analysis or heat mapping.

2.8. Resazurin reduction assay

The resazurin reduction assay was conducted to measure the inhibition of cancer cell lines by selected compounds. The assay was performed as previously described (Adham et al., 2021).

3. Results

3.1. Overview of sideritis components library

By literature mining and extracting the components of the genus *Sideritis*, we generated a phytochemical library containing 657 secondary plant metabolites. The compounds were classified based on their chemical structures. As shown in Fig. 1A, one third of all compounds belonged to diterpenes (33%), one third were phenolic structures (32%), and the rest belonged to other types of terpenes (mono-, sesqui- and triterpenoids), sterols, and straight aliphatic chains (35%).

There were 218 diterpenes contained in the *Sideritis* genus. Of them, 98 were kaurenes (45 %), 59 were labdanes (27 %), 26 were beyeranes (12 %), 9 were abietanes (4 %), 8 were atisanes (8 %), 7 were pimaranes (3 %), 7 were trachylobanes (3 %), 2 were rosanes (1 %), and 2 were other types of diterpenes (1 %) (Fig. 1B).

The number of phenolics in the *Sideritis* genus was 211. Of them, 131 were flavonoids and their derivatives (62 %), 51 were simple phenols (24 %), 15 were phenylethanoids and phenylpropanoids (7 %), 7 were coumarins (3.5 %), and 7 were lignans (3.5 %) (Fig. 1C).

A total of 82 sesquiterpenes were found in the *Sideritis* genus, and 12 of them were eudesman-type sesquiterpenes. Sixty-three monoterpenes were constituents of the essential oils, and 15 of them were iridoids. There were 32 triterpenes, and lastly, 53 aliphatic structures (Fig. 1D).

3.2. Virtual screening and molecular docking

Virtual screening and molecular docking represent important computational chemistry techniques utilized for rational drug design. The chemical *Sideritis* library consisting of 657 compounds was first screened by PyRx for binding affinities to both NLRP3 and NF-κB proteins. The top 120 compounds for both proteins were selected for further investigation. The structures of the top 120 compounds were quite different, depending on the protein which they bound to. While diterpenes constituted the largest number of compound interactions with NLRP3, phenolic structures represented the majority of NF-κB-binding compounds (Tables S3 and S4).

Then, each of the subsets with the top 120 compounds for NLRP3 and NF-κB were docked using AutoDock 4.2.6. The compounds were grouped into affinity ranges based on their predicted binding energies towards NLRP3 protein as shown in Fig. 2A. The largest percentage of compounds (36.7%) fell within the moderate affinity range of −9.9 to −9 kcal/mol. The next largest group (17.5%) displayed slightly stronger affinities in the −10.9 to −10 kcal/mol range. A smaller but still substantial subset (15%) exhibited weaker affinities from −8.9 to −8 kcal/mol. Notably, 11.7% of all compounds demonstrated the highest affinities, between −11.9 and −11 kcal/mol. In summary, the majority of the analyzed compounds (69.2%) had moderate to strong predicted NLRP3 binding affinities between −10.9 and −8 kcal/mol. The top 120 compounds for the NF-κB protein were ranked based on their prediction affinities. The largest group, making up 28.3% of the 120 compounds, displayed moderate predicted affinities from −8.9 to −8 kcal/mol. The next major subset (19.1%) showed slightly stronger predicted affinities, ranging from −9.9 to −9 kcal/mol. An additional 15.3% of the compounds had weaker predicted affinities between −7.9 and −7 kcal/mol. In total, most of the top-ranking compounds (62.7%) exhibited moderate to relatively strong NF-κB binding affinities *in silico* between −9.9 and −7 kcal/mol (Fig. 2B).

Linear regression correlations of LBE and predicted binding constants of each of the top 120 compounds are shown in Fig. 3, indicating

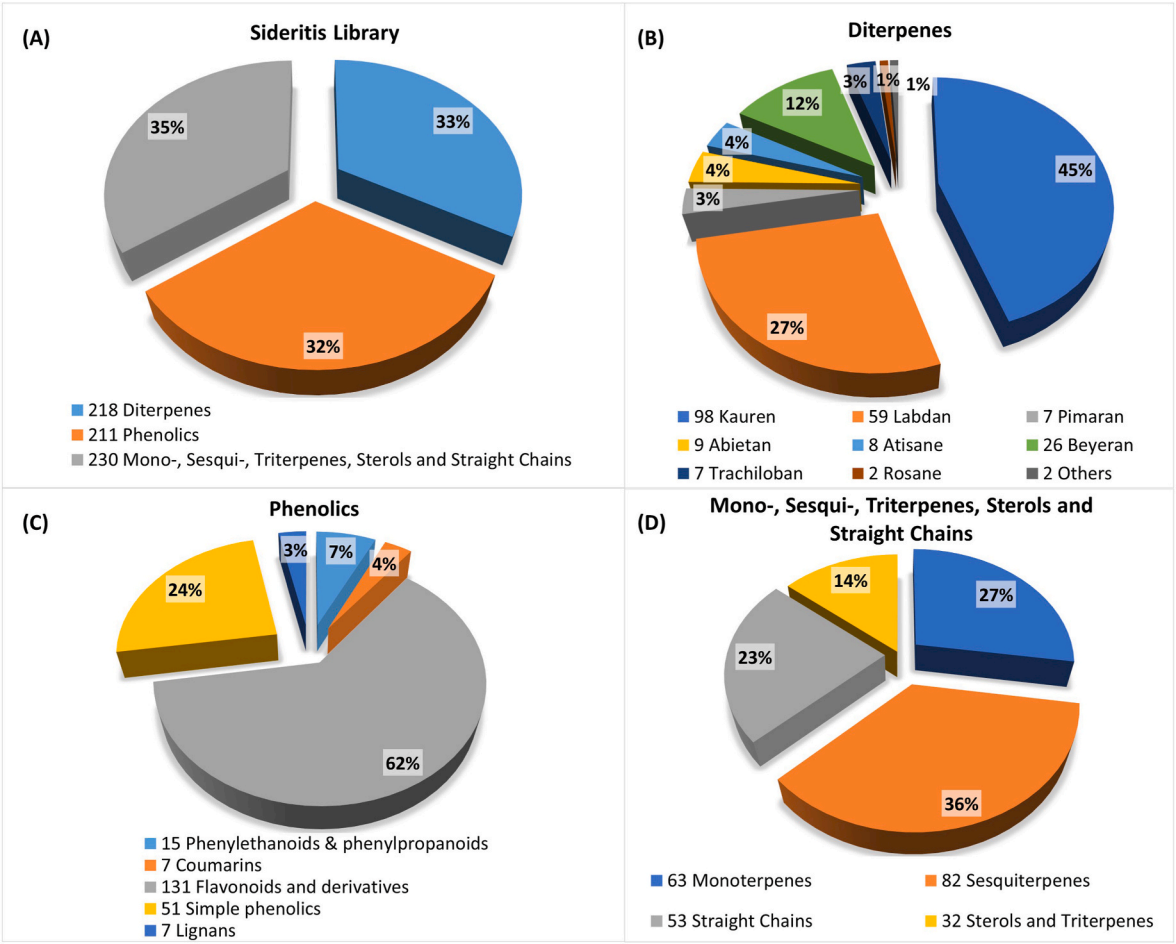

Fig. 1. Phytochemical library was formed by mining the published literature on the genus *Sideritis*. (A) The main three categories of *Sideritis* genus components. Diterpenes made about one-third of the chemicals (33%), followed by phenolic structures (32%), other terpene types (mono-, sesqui-, and triterpenoids), sterols, and straight aliphatic chains (35%). (B) The 218 diterpenes from *Sideritis* plants were categorized based on their chemical structures. The most common were kaurenes (45%), labdanes (27%), and beyeranes (12%). Together these three groups accounted for 84% of the total diterpenes. The remaining 16% included smaller numbers of abietanes, atisanes, pimaranes, trachylobanes, rosanes, and other diterpenes. (C) The study examined 211 phenolic compounds from *Sideritis* plants. Making nearly 62% of the total, flavonoids and their derivatives constituted the largest group. Phenylethanoids and phenylpropanoids (7%) and simple phenols (24%) were the other two main phenolic groupings. Coumarins (3.5%) and lignans (3.5%) were minor groupings. (D) The study identified 82 total sesquiterpenes in *Sideritis* plants. The main sesquiterpene subgroup was eudesmanes, with 12 compounds. For monoterpenes, 63 compounds were found in essential oils, including 15 iridoids. In addition, there were 32 triterpenes and 53 aliphatic compounds characterized in *Sideritis* genus.

that inhibition constants (Ki) are consistent with LBE values.

The top 10 compounds with the highest binding affinities are depicted in Table 1 for NLRP3 and in Table 2 for NF-κB. The lowest binding energy (LBE) of verbascoside was −14.3 ± 0.5 kcal/mol for NLRP3 with a predicted inhibition constant (pK_i) of 0.042 ± 0.033 nM and a LBE of −10.39 ± 0.12 kcal/mol and a pK_i of 0.024 ± 0.005 μM for NF-κB. Apigenin 7-,4′-bis(trans-*p*-coumarate) had a binding energy of −14.5 ± 0.5 kcal/mol for NLRP3 with a pK_i value of 0.024 ± 0.005 nM. Phenolic structures displayed better binding affinities compared to terpenoid structures. Although only 22.5 % of the 120 compounds binding to NLRP3 were phenolics, exclusively phenolic structures were among the top 10-ranked phytochemicals (100 %) based on binding affinity. For both proteins, phenylethanoid and their glycosides as well as flavonoid derivatives lined up among the top 10 compounds. NLRP3 and NF-κB had 7 compounds in common within the top 10, which were verbascoside, isoverbascoside, apigenin-7-,4′-bis-(trans-*p*-coumarate), martynoside, forsythoside A, apigenin-7-(6″-*p*-coumaroyglucoside), and 1-rhamnosyl-1-coumaroyl-3-dihydrocaffeoyl-5-protocatechuoyl tetraester of quinic-acid. Since verbascoside and isoverbascoside were among the most abundant compounds in *Sideritis* plants (Sarikurkcu et al., 2020; Ververis et al., 2023; Goulas et al., 2014), these two compounds were chosen for further experiments, as well asapigenin 7-,4′-bis(trans-*p*-coumarate) as it also appeared in the top 10 lists for both proteins.

Molecular interactions of the chosen compounds against the two proteins are depicted in Table 3, while the interaction sites are shown in Fig. 4. For both proteins, verbascoside and the positive controls shared the same binding area.

3.3. LC-HRMS analysis

LC-HRMS determination was made in PE, DCM, EtOAc and BuOH extracts obtained by liquid-liquid extraction of *S. stricta* plant, and 22 substances were analyzed. Comparing the four extracts, the EtOAc extract was the richest in terms of the content of the substances in the library, followed by the BuOH extract. As expected, the PE extract was lower in phenolic substances than other extracts. Verbascoside was the most abundant compound in all three extracts, 62.26 g/kg in the EtOAc extract, 31.02 g/kg in the BuOH extract, and 11.67 g/kg in the PE extract of *S. stricta*. Chlorogenic acid was the second most prevalent compound for BuOH (19.26 g/kg), EtOAc (18. 80 g/kg) and PE (7.22 g/kg) extracts of the plant. The DCM extract was rich in vanillic acid

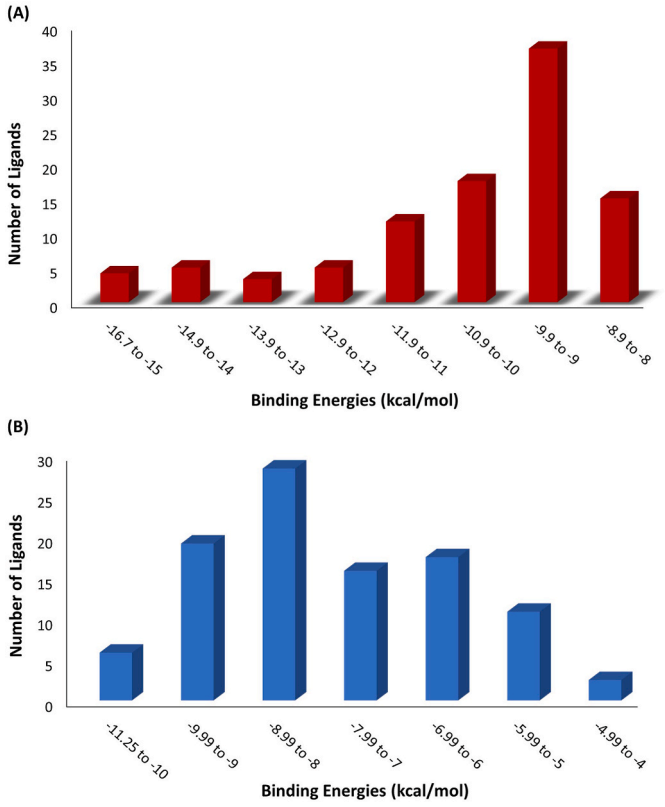

Fig. 2. Docking rankings of the top 120 compounds which were taken from the top results of PyRx screening of *Sideritis* components library for NLRP3 and NF-κB. **(A)** The compounds were ranked based on their predicted affinity for the NLRP3 protein. The largest group (36.7%) had predicted affinities between −9.9 and −9 kcal/mol. The second largest group (17.5%) had affinities between −10.9 and −10 kcal/mol. The third largest group (15%) had weaker affinities between −8.9 and −8 kcal/mol. A smaller group (11.7%) had even stronger predicted affinities between −11.9 and −11 kcal/mol. Overall, the majority of compounds (69.2%) had predicted NLRP3 affinities between −10.9 and −8 kcal/mol. **(B)** The top 120 compounds were ranked by their predicted binding affinity to the NF-κB protein. The largest percentage (28.3%) had moderate predicted affinities ranging from −8.9 to −8 kcal/mol. The next largest group (19.1%) displayed slightly stronger predicted affinities between −9.9 and −9 kcal/mol. Another sizeable subset (15.3%) showed weaker affinities in the range of −7.9 to −7 kcal/mol. In summary, the majority of the top 120 compounds exhibited moderate predicted NF-κB binding affinities between −9.9 and −7 kcal/mol.

(19.62 g/kg), p-coumaric acid (18.16 g/kg), and salicylic acid (14.39 mg/kg) (Table 4).

3.4. Microscale thermophoresis

Microscale thermophoresis (MST) is a potent tool for measuring biomolecular interactions. The technique relies on the directed movement of molecules along a temperature gradient. Based on the results of the docking analysis, commercial availability, and abundance in the plant, verbascoside, isoverbascoside, and apigenin 7,4′-bis(trans-*p*-coumarate) were subjected to MST for both NLRP3 and NF-κB. As shown in Fig. 5, verbascoside had a K_d value of 0.67 ± 0.18 μM and apigenin 7-,4′-bis(trans-*p*-coumarate) of 4.60 ± 1.66 μM for NLRP3. Interestingly isoverbascoside, the isomer of verbascoside, did not bind to NLRP3, underlining the relevance of isomerism for binding to target proteins. For NF-κB, verbascoside had a K_d value of 0.01 ± 0.08 μM and apigenin 7,4′-bis(trans-*p*-coumarate) of 0.27 ± 0.75 μM. No binding interaction was observed between isoverbascoside and NF-κB. These binding kinetics of MST are shown in Fig. 6.

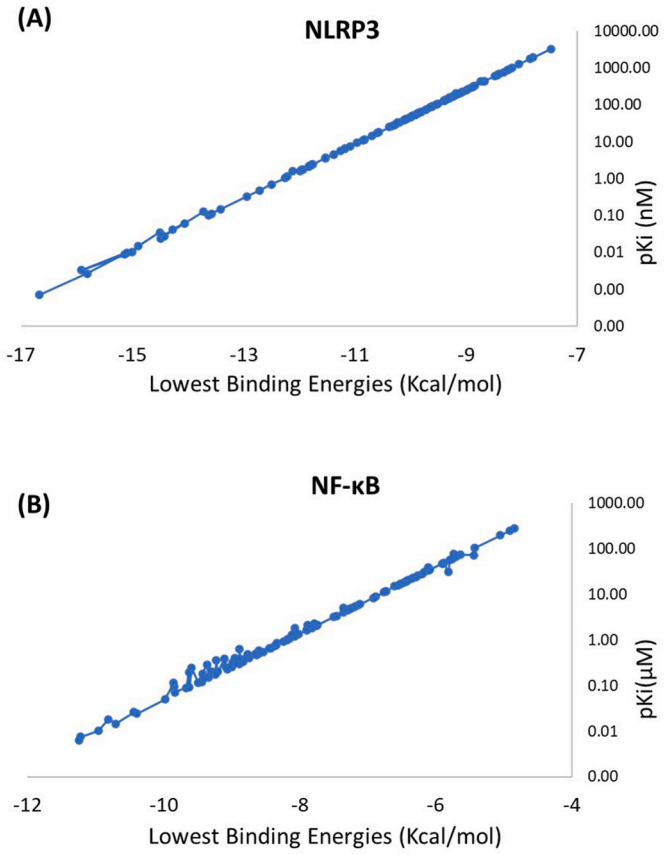

Fig. 3. Linear regression correlation of lowest binding energies (LBE) and pKi values for two proteins and 120 compounds. The horizontal axis is depicted as a logarithmic scale. **(A)** Linear regression correlation for NLRP3 protein **(B)** Linear regression correlation for NF-κB protein.

Table 1
Lowest binding energies and estimated inhibition constants of top 10 compounds from docking results toward NLRP3 protein.

	Compounds	LBE [kcal/mol]	pKi (nM)
1.	1-Rhamnosyl, 1-coumaroyl, 3-dihydrocaffeoyl, 5-protocatechuic tetraester of quinic acid	−15.9 ± 1.9	0.0033 ± 0.0036
2.	Lavandulifolioside	−15.8 ± 0.2	0.0027 ± 0.0009
3.	Isoverbascoside	−15.1 ± 0.4	0.0091 ± 0.0054
4.	Apigenin-7-(3″-*p*-coumaroyglucoside)	−15.0 ± 0.0	0.0101 ± 0.0003
5.	Apigenin-7-(6″-*p*-coumaroyglucoside)	−14.9 ± 0.5	0.0148 ± 0.0094
6.	Forsythoside A	−14.5 ± 0.6	0.0351 ± 0.0391
7.	Apigenin 7-,4′-bis(trans-*p*-coumarate)	−14.5 ± 0.1	0.0244 ± 0.0055
8.	Ozturkoside A	−14.4 ± 1.0	0.0275 ± 0.2566
9.	Verbascoside	−14.3 ± 0.5	0.0424 ± 0.0327
10.	Martynoside	−14.1 ± 0.5	0.0609 ± 0.0511
	Mcc950 (control)	−11.4 ± 0.0	4.5133 ± 0.0252

*All data are mean ± SD of triplicate measurement.

Table 2
Lowest binding energies and estimated inhibition constants of top 10 compounds from docking results toward NF-κB protein.

	Compounds	LBE [kcal/mol]	pKi (μM)
1.	Apigenin-7-(6″-*p*-coumaroyglucoside)	−11.25 ± 0.33	0.0063 ± 0.0034
2.	Apigenin-7-,4′-bis-(trans-*p*-coumarate)	−11.22 ± 0.46	0.0075 ± 0.0063
3.	Forsythoside A	−10.96 ± 0.31	0.0102 ± 0.0052
4.	Pentagalloyl glucose	−10.81 ± 0.69	0.0184 ± 0.0197
5.	Isoverbascoside	−10.7 ± 0.13	0.0146 ± 0.0030
6.	1-Rhamnosyl-1-coumaroyl-3-dihydrocaffeoyl-5-protocatechuoyl tetraester of quinic-acid	−10.43 ± 0.38	0.0261 ± 0.0180
7.	Verbascoside	−10.39 ± 0.12	0.0243 ± 0.0047
8.	Hypolaetin-7-*O*-[6‴-*O*-acetyl]-allosyl-(1 → 2)-[6″-*O*-acetyl]-glucoside	−9.85 ± 0.90	0.1140 ± 0.1336
9.	Martynoside	−9.84 ± 0.71	0.0969 ± 0.1084
10.	Echinacoside	−9.84 ± 0.42	0.0717 ± 0.0464
	Hu-211 (control)	−8.99 ± 0.50	23.0000 ± 0.3323

*All data are mean ± SD of triplicate measurement.

Table 3
Amino acid interactions of the selected 9 candidates to NLRP3 and NF-κB as predicted by AutoDock 4.2.6.

Compounds	NLRP3 amino acid interactions	NF-κB amino acid interactions
Apigenin 7-,4′-bis (trans-*p*-coumarate)	Thr167, Leu169, Lys230, Ile232, Arg235, Thr347, Leu411, Phe506, Ile519, His520	Lys90, Asp94, Leu95, Ala104, Leu109, Ser115, Glu116, Leu117, Gly118, Ile119, Lys153, Gln157, Arg160
Verbascoside	Ile149, Glu150, Leu162, Arg165, Tyr166, Thr167, Leu169, Gly227, Ile232, Tyr379, Pro410, His520	Asp94, Leu95, Arg103, Ala104, Leu117, Gly118, Ile119, Lys153, Arg160, Ser161, Phe197, Ser206.
MCC950 (positive control)	Glu150, Leu169, Gly227, Ile228, Gly229, Ile232, Leu233, Phe371, Tyr379, Trp414, His520	
HU-211 (positive control)		Glu91, Leu95, Ala104, Leu117, Ile119, Lys153, Arg156, Arg160

3.5. Anti-cancer activity of verbascoside

The first part of our investigation pointed to verbascoside as an interesting compound inhibiting NF-κB and NLRP3. Verbascoside belongs to the group of caffeoyl phenylethanid glycosides (Fig. 7A and B). Since both target proteins are not only involved in inflammatory processes but also in cancer development (Grivennikov et al., 2010; Zhiyu et al., Afonina et al., 2017; Khandia and Munjal, 2020), we were interested in studying the anticancer activity of verbascoside. For this reason, we mined the repository of the National Cancer Institute's drug screening program (https://dtp.cancer.gov) and found that 49 cell lines of different tumor origin have been tested for their responsiveness to verbascoside. We calculated the mean values of the tumor cell lines belonging to each of the tumor types. Leukemia cell lines were most sensitive to verbascoside, while lung cancer lines were most resistant. The other cancer types were of intermediate responsiveness (carcinomas of the colon, ovary, breast, prostate and kidney as well as melanomas and brain tumors) (Fig. 7C).

A correlation study was performed between the $\log_{10}IC_{50}$ values of 49 verbascoside-treated cell lines and those treated with 81 common

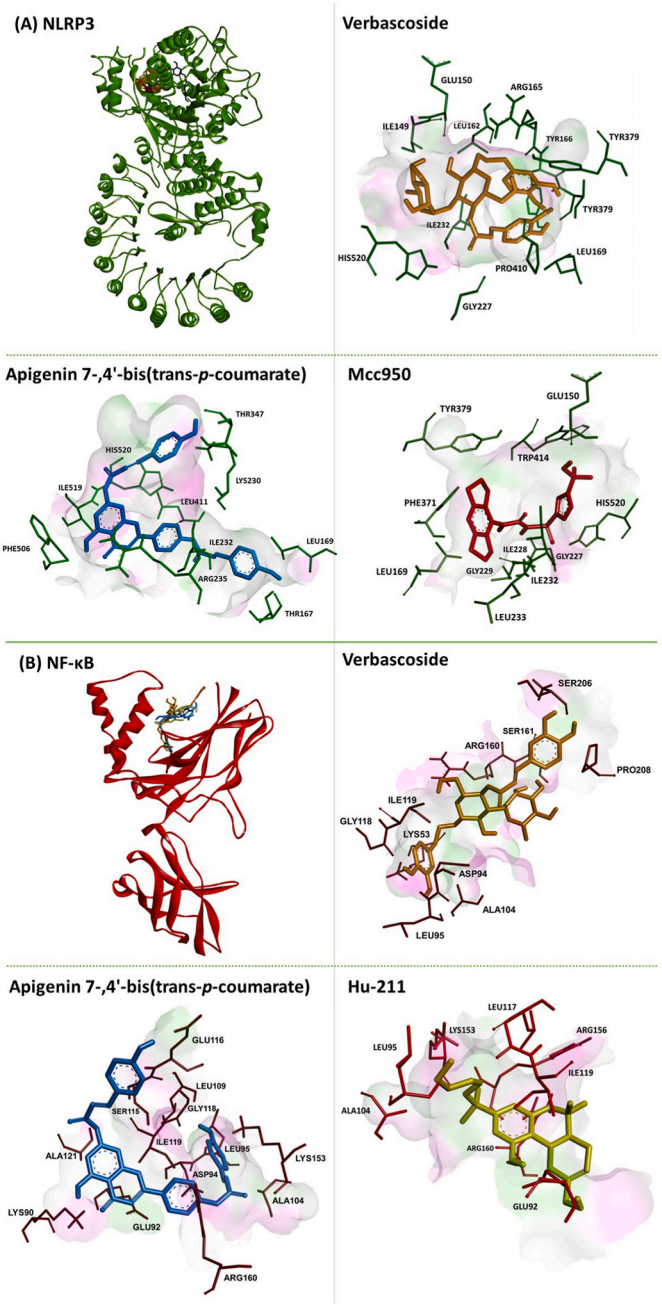

Fig. 4. Molecular docking poses and interacting surfaces between the two proteins and ligands. **(A)** NLRP3 protein (pdb: 6npy) interacting amino acid residues with verbascoside, apigenin 7-,4′-bis(trans-*p*-coumarate), and the positive control Mcc950 **(B)** NF-κB protein (pdb: 1a3q) interacting amino acid residues with verbascoside, apigenin 7-,4′-bis(trans-*p*-coumarate), and the positive control Hu-211.

anticancer compounds, each of which has a distinct and well-characterized mechanism of action aiming to gain deeper insights into the possible anticancer mechanisms of verbascoside. The results showed a strong correlation between verbascoside and several common anticancer drug types. There was a high correlation between verbascoside and 10 out of 16 alkylating agents, or 63% of this class (Fig. 7D), implying that verbascoside, like alkylating chemicals, may harm DNA in cancer cells. Furthermore, the responsiveness of some DNA topoisomerase I or II inhibitors, as well as antimetabolites, was also associated with verbascoside (Fig. 7D). Correlations were also found between some antihormones and tyrosine kinase inhibitors to verbascoside, which

Table 4
The quantity (mg/kg extract) of phenolic compounds in *S. stricta* extracts determined by LC-HRMS chromatograms.

Madde Adı	RT	SS-PE	RT	SS-DCM	RT	SS-EtOAc	RT	SS-BuOH	U %
Ascorbic acid	2.12	129.30	2.15	125.04	2.17	40.67	2.17	32.69	3.94
Chlorogenic acid	2.50	7222.01	2.49	3451.93	2.49	18795.35	2.50	19263.92	3.58
Verbascoside	2.95	11671.16	2.94	3946.26	2.96	62273.74	2.97	31015.36	2.93
Caffeic acid	3.17	123.55	3.16	185.10	3.17	816.61	3.18	65.81	3.74
Vanilic acid	4.09	524.07	4.09	19617.69	4.08	1042.16	–	<LOD	3.49
Luteolin 7-glucoside	–	<LOD	–	<LOD	–	<LOD	–	<LOD	4.14
p-Coumaric acid	4.19	2276.63	4.19	18164.59	4.20	7678.22	4.21	935.84	3.31
Rutin	4.56	990.64	4.56	248.09	4.58	642.78	4.59	1689.96	3.07
Hyperoside	–	<LOD	–	<LOD	–	<LOD	–	<LOD	3.46
Apigenin 7-glucoside	5.06	3.78	6.12	1.49	5.05	22.95	5.06	8.87	3.59
Quercetin	5.28	5.38	5.29	8.06	5.29	90.70	5.27	12.60	2.95
Salicylic acid	5.81	515.17	5.81	14393.50	5.77	534.56	5.77	261.76	1.89
Nepetin	5.77	16.02	5.76	93.49	5.73	194.06	5.68	21.07	2.19
Kaempferol	5.83	8.49	5.83	12.04	5.77	55.96	–	<LOD	3.56
Apigenin	6.20	3.17	6.20	7.29	6.25	19.74	6.22	0.66	2.87
Chrysin	7.06	1.34	7.12	27.42	7.03	1.73	7.11	0.26	3.24
Acacetin	7.26	61.10	7.29	3046.55	7.24	185.76	7.23	4.21	3.98
Homogentisic acid	–	<LOD	2.41	152.78	2.39	212.43	2.21	39.93	4.35
3,4-Dihydroxybenzaldehyde	2.97	7.33	2.98	76.11	2.98	23.30	3.01	1.75	3.79
Hispidulin 7-glucoside	5.08	295.52	5.09	104.53	5.07	2794.68	5.08	1609.64	4.57
Apigenin 7-O-acylglucoside	–	<LOD	–	<LOD	–	<LOD	–	<LOD	2.70
Apigenin 7-metilat	7.26	8.05	7.29	395.16	7.24	24.33	7.23	0.57	2.94

RT: Retention time, LOD: Limit of detetion, SS: *Sideritis stricta*, PE: Petrol etherium, DCM: Dichloromethane, EtOAc: Ethyl acetate, BuOH: Butanol.

were not further followed up.

The oncobiogram shown in Fig. 7E presents particular *r*-values reflecting the intensity and importance of the relationship between the 10 alkylating agents (busulfan, estramustine, melphalan, chlorambucil, streptozocin, bendamustine, semustine, lumistine, carmustine, thiotepa) and verbascoside in the NCI panel. This comprehensive graphical illustration demonstrates strong relationships and offers a visual aid for comprehending the potential DNA-damaging effects of verbascoside.

3.6. Classical modes of drug resistance

The efficacy of many established anticancer drugs is diminished by the development of resistance which leads to the failure of chemotherapy and the death of patients. Therefore, it is imperative to identify compounds which are not involved in the common drug resistance phenotypes. We correlated the $\log_{10}IC_{50}$ values of verbascoside with the parameters of multidrug resistance-mediating ATP-binding cassette transporters (ABCB1, ABCB5, ABCC1, and ABCG2), oncogenes and tumor suppressors (EGFR, TP53, NRAS), other resistance genes (HSP90, GSTP1), and cellular proliferation (cell doubling times). The parameters were protein expression (Western blotting, protein array), mRNA expression (microarray hybridization, RT-PCR, Northern blotting), mutation analysis (cDNA sequencing), and functional assays (drug uptake assays, yeast functional assays). Table 5 shows the correlation coefficients (*r*-values) and significance levels (*p*-values) for the obtained results. The analysis presents that none of the expression patterns or mutations examined exhibited a significant correlation with verbascoside, except *NRAS* mutations (which had a significant negative correlation with an *r*-value of −0.652 and a *p*-value of 6.11×10^{-7}). The positive controls, on the other hand, showed a strong correlation with these resistance mechanisms. These findings show that verbascoside is not involved in classical drug resistance mechanisms typically mediated by ABC transporters, oncogenes, tumor suppressors, other resistance genes, or cellular proliferation rates. The lack of significant correlation implies that verbascoside may continue to be effective and can evade common resistance mechanisms even in situations where cancer cells have become resistant to previous therapies.

3.7. Cytotoxicity of verbascoside in sensitive CCERF-CEM and multidrug-resistant CEM/ADR5000 leukemia cells

For exemplary validation of the correlation analyses using the NCI cell line panel, we treated CCRF-CEM and P-glycoprotein (ABCB1)-overexpressing CEM/ADR5000 cells with verbascoside. The IC_{50} value of verbascoside was 13.8 ± 1.9 μM in sensitive CCRF-CEM cells and 46.4 ± 4.6 μM in multidrug resistant CEM/ADR5000 cells. Thus, the degree of resistance was approximately 3-fold. IC_{50} value of doxorubicin was 0.051 ± 0.006 μM in CCRF-CEM cells and 20.1 ± 2.6 μM in CEM/ADR5000 cells (degree of resistance: 400-fold) (Fig. 8).

3.8. Proteomic profiling of verbascoside

Since most of the classical mechanisms of drug resistance were not operative in the case of verbascoside, but the $\log_{10}IC_{50}$ values were considerably different between the panel of 49 cell lines (range from −6.198 M to −4.0 M), it is obvious that the response of these cell lines towards verbascoside was regulated by other proteins than the classical drug resistance mechanisms. Therefore, we took advantage of the expression profiling of 3171 proteins in these cell lines by mass spectrometry (Guo et al., 2015). The protein expression values were associated with the $\log_{10}IC_{50}$ values for verbascoside using the Pearson correlation test. The top 20 directly, and the top 20 inversely correlating proteins were taken and subjected to hierarchical cluster analysis and heatmap generation. It can be assumed that protein expressions directly correlating with the $\log_{10}IC_{50}$ values (*i.e.*, high expression levels correlate with high $\log_{10}IC_{50}$ values) may contribute to resistance of cell lines to this compound, while inversely correlating protein expressions (*i.e.*, low protein expressions correlate with high $\log_{10}IC_{50}$ values), may act as factors determining sensitivity towards verbascoside. Subjecting these 40 proteins to Ward-based cluster analyses resulted in the heatmap shown in Fig. 9. Each two main clusters were obtained for the 40 proteins (clusters A and B) and for the 49 cell lines (clusters 1 and 2).

As a next step, we used the $\log_{10}IC_{50}$ values for verbascoside which previously had not been included in the analysis, and correlated them with the verbascoside responses of cell lines in clusters 1 and 2. Individual $\log_{10}IC_{50}$ values greater than the median value of all cell lines were defined as resistant and those with smaller values than the median, as sensitive. As shown on the right side of Fig. 9, cell lines with stronger verbascoside-resistance were preferentially assembled in cluster 1 by the

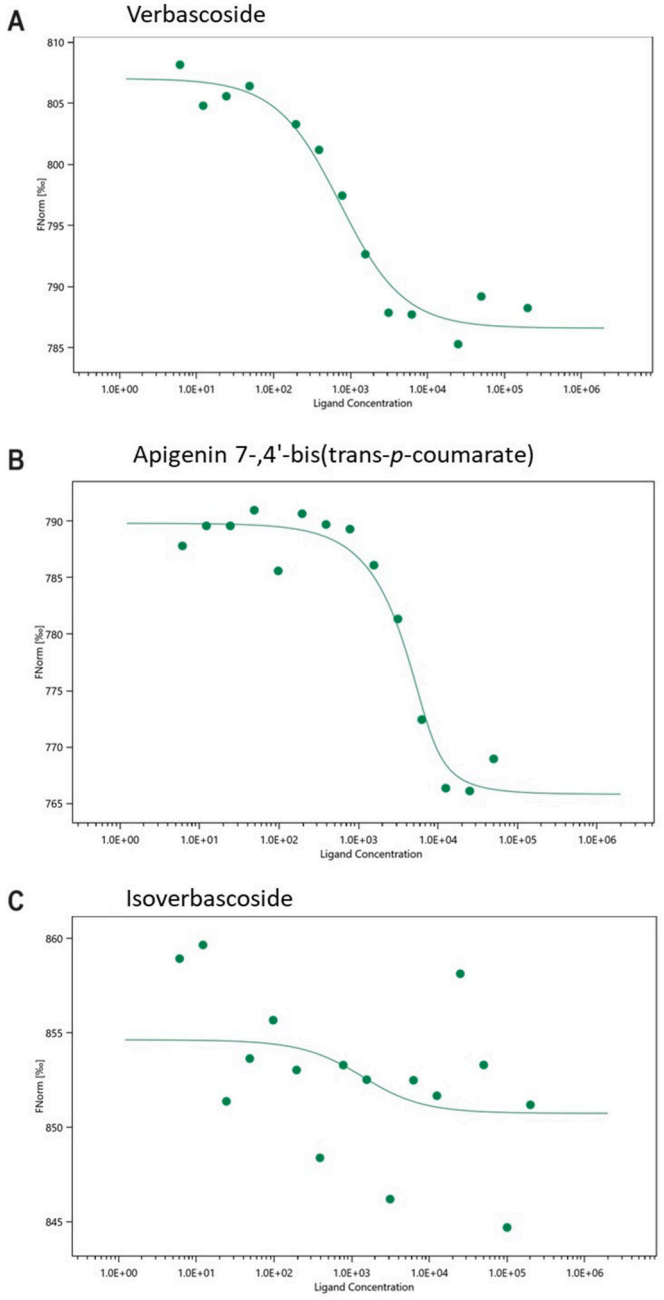

Fig. 5. Microscale thermophoresis of three candidate compounds to NLRP3 and (A) verbascoside, (B) apigenin 7-,4′-bis(trans-*p*-coumarate), and (C) isoverbascoside.

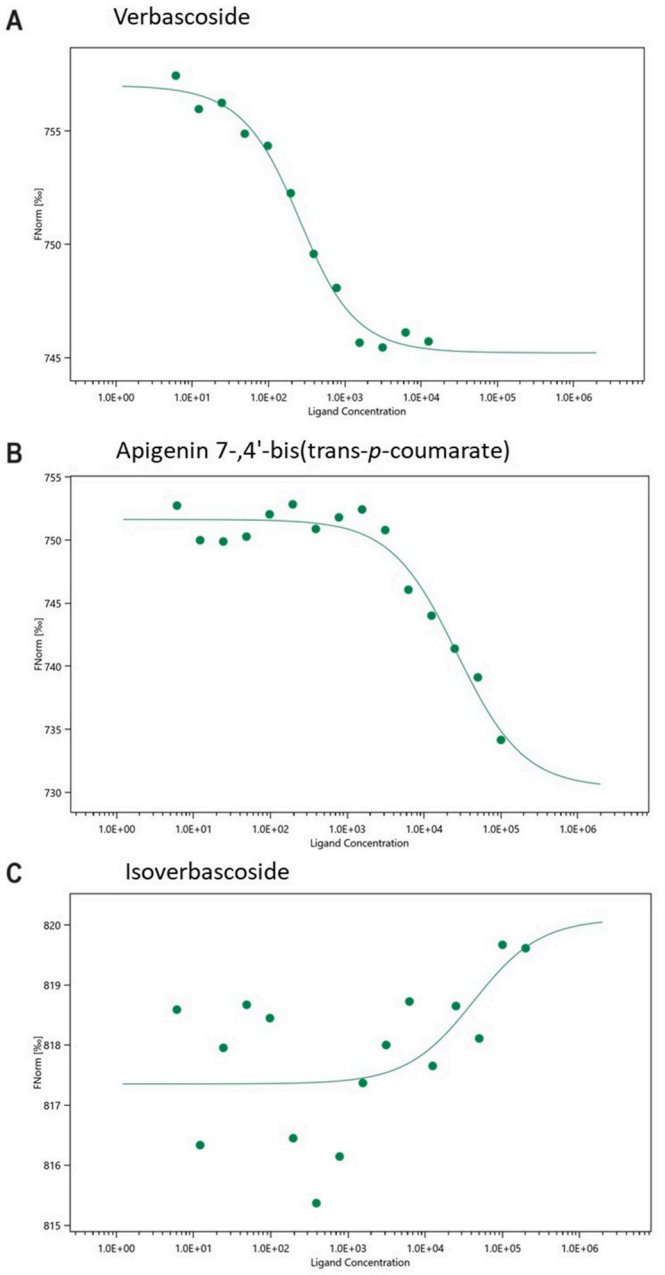

Fig. 6. Microscale thermophoresis of three candidate compounds to NF-κB and (A) verbascoside, (B) apigenin 7-,4′-bis(trans-*p*-coumarate), and (C) isoverbascoside.

cluster analyses algorithm, while verbascoside-sensitive ones were found in cluster 2. We calculated this distribution by the chi2 text and found a significant relationship ($p = 0.001$; bottom of Fig. 9). This result indicates that the expression profile of these 40 proteins can predict the sensitivity and resistance of the NCI cell line panel to verbascoside.

4. Discussion

Sideritis species have been utilized as medicinal herbs in traditional medicine in Mediterranean regions, Central Europe, and the Near East for centuries. The aerial parts of the herb were commonly consumed as tea prepared by decoction or infusion which are rich in polyphenolic compounds. Various pharmacological activities were reported for different species of the *Sideritis* genus (Aneva et al., 2019; González-Burgos et al., 2011), including its anti-inflammatory activity (Güvenç et al., 2010; Cavalcanti et al., 2021).

In this study, we constructed a chemical library for *Sideritis* species containing 657 secondary metabolites. Like many other plants, this genus is rich in terpenoids, especially diterpenes, and almost half of them have a kaurene skeleton. One-third of the library comprises phenolic structures, and more than half of them are flavonoids and their derivatives. Previous phytochemical profiling studies showed that *Sideritis* species are abundant in derivatives of hypolaetin and isoscutellarein (Menković et al., 2010). The remaining third part contains other types of terpenoids with sterols and aliphatic molecules. The library compounds were then subjected to virtual screening for binding to NLRP3 and NF-κB. The top-rated 120 compounds for each protein from the virtual drug screening with PyRx were examined with molecular docking using AutoDock 4.2.6. If we inspect the chemical structures of

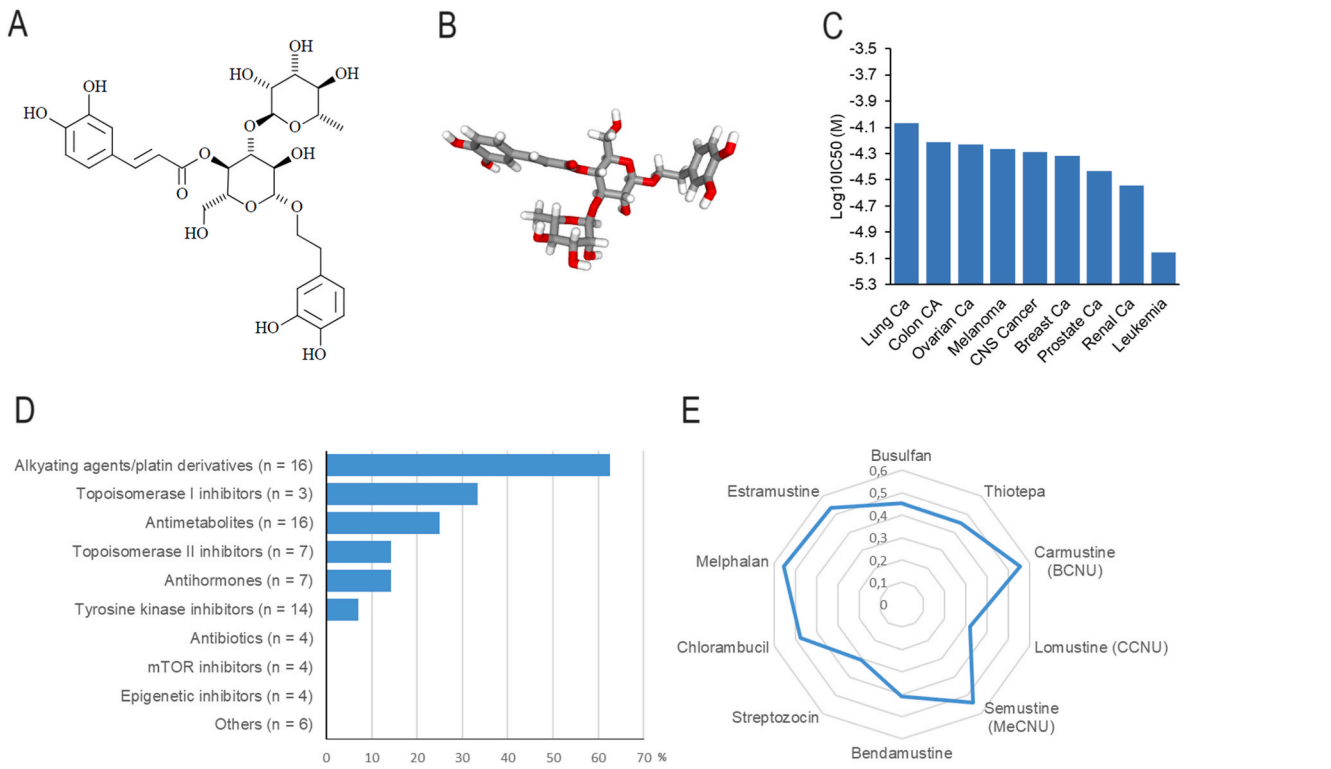

Fig. 7. Tumor type and drug class profiling to verbascoside (A, B) Chemical 2D and 3D structures of verbascoside. The 2D structure has been taken from Wikipedia, the 3D structure from PubChem); (C) Tumor type-specific profiling of the NCI tumor cell lines. Shown are the mean values of cell lines belonging to the different tumor types displayed; (D) Drug class-specific profiling of the NCI tumor cell lines. The drug panel consisted of 81 standard anticancer drugs with the modes of actions displayed. (E) Oncobiogram of alkylating anticancer agents whose $\log_{10}IC_{50}$ values in the NCI panel significantly correlated with those of verbascoside. Shown are the correlation coefficients (*r*-values).

the compounds common in both tables with the top 10 candidates, we see that they are under the umbrella of phenolic structures, *i.e.*, flavonoids and their glycosides, and phenylethanoids. Phenolics usually consist of a benzene ring with one or more hydroxyl groups, enabling them to form various interactions, including hydrophobic, π-π, and hydrogen bond interactions. Because of their structural adaptability, they can fit into many protein-active sites. Phenylethanoid glycosides have two moiety types: phenolic and glycoside (sugar-containing). In the protein's active site, the glycoside portion can form hydrogen bonds with polar residues or water molecules, while the phenolic portion can participate in hydrophobic and π-π stacking interactions. Flavonoids, with their two aromatic rings (A and B) and a pyran ring (C), can engage in multiple types of interactions such as hydrogen bonds, hydrophobic interactions π-π stacking, and metal coordination. Therefore, all three groups can adopt different binding modes as they have several functional groups. Certain phenolic compounds and glycosides have some degree of flexibility, enabling them to fit into various protein binding locations. Their flexibility may allow them to interact with many targets. Many proteins have a flexible binding site. The adaptability of these sites makes it possible for various compounds to bind effectively.

Phenylethanoid and phenylpropanoid glycosides were the most abundant type of compounds in *Sideritis* species constituting about 50% of the total phenolic content, with the highest quantities for lavandulifolioside and verbascoside (Stanoeva et al., 2015). Our LC-HRMS analysis also demonstrated the plant's abundance of verbascoside. Verbascoside, a prevalent compound in the plant kingdom, is a common type of disaccharide caffeoyl ester and has mostly been identified in plants of the *Verbascum* genus but has also been found in more than 200 other plant species from 23 different plant families. Verbascoside, also known as acteoside, exhibits a broad range of biological activities (Alipieva et al., 2014; Xiao et al., 2022). Verbascoside decreased elevated levels of inflammatory mediators (NLRP3, NF-κB, TNF-α, and IL-1β) in the intracerebral hemorrhage (ICH) mouse model. The neuroprotective effect of verbascoside was dependent on the presence of NLRP3, since verbascoside was inactive in NLRP3 knockout mice (Zhou et al., 2021). Treatment with verbascoside decreased the expression of inflammasome and caspase-1 proteins in a mouse model of LPS-induced septic cardiomyopathy (Zhu et al., 2022). Verbascoside was well tolerated after both single and chronic administration without toxicity or fatalities in animals at LD_{50} dose higher than 5 g/kg. In subacute toxicity studies, no significant differences were detected between the control and treatment groups at doses of 0, 20, 30 mg/kg for an administration period of 21 days (Etemad et al., 2015).

Apigenin derivatives were in the group of top 10 compounds with low binding energies for both proteins. Other *in silico* studies on apigenin derivatives also showed strong hydrogen bonding on the main protease of SARS-CoV-2 (Farhat et al., 2022). Apigenin 7-,4′-bis(trans--*p*-coumarate) was first isolated from *S. syriaca* (Plioukas et al., 2010). To the best of our knowledge, no bioactivity studies of this compound have been reported yet. Therefore, we also chose apigenin 7-,4′-bis(trans--*p*-coumarate) for our analyses.

Microscale thermophoresis experiments revealed that verbascoside bound with high affinities to both proteins of interest with K_d values of 0.67 ± 0.18 μM and 0.01 ± 0.08 μM. These findings are supported by data in the literature (Zhou et al., 2021; Zhu et al., 2022). Interestingly, the isomer isoverbascoside did not show any binding to NLRP3 and NF-κB proteins. Verbascoside and isoverbascoside have very similar structures, the main difference being the binding position of the caffeoyl group to the glucose moiety. In verbascoside, the caffeoyl group is bound at the 4th position of glucose, whereas in isoverbascoside, the caffeoyl group binds to the 6th position of glucose. This small structural difference in the binding orientation of the caffeoyl group is what distinguishes verbascoside from isoverbascoside. The remaining structures of the two molecules are identical. To our knowledge, there is no

Table 5
Involvement of classical drug resistance mechanisms in the response of 49 NCI tumor cell lines to verbascoside. The $\log_{10}IC_{50}$ values of verbascoside have been correlated to the expression, function, and mutation status of ATP-binding cassette transporters (*ABCB1, ABCB5, ABCC1, ABCG2),* oncogenes and tumor suppressors (*EGFR, TP53, NRAS*), other resistance-related proteins (*HSP90, GSTP1*), and cellular proliferation (cell doubling time of cell lines). Positive control drugs for the respective drug resistance phenotypes have been shown here for comparison and were taken from Saeed et al. (2018a, 2018b) and Khalid et al. (2022).

		Verbascoside ($\log_{10}$ IC_{50}, M)	Control Drug ($\log_{10}$ IC_{50}, M)
ABCB1 Expression			Epirubicin
7q21 (Chromosomal	*r*-value	0.125	[a]**0.447**
Locus of *ABCB1* Gene)	*p*-value	0.212	[a]**3.55×10^{-4}**
ABCB1 Expression	*r*-value	1.126	[a]**0.533**
(Microarray)	*p*-value	0.0196	[a]**6.82×10^{-6}**
ABCB1 Expression	*r*-value	−0.035	[a]**0.410**
(RT-PCR)	*p*-value	0.413	[a]**1.54×10^{-3}**
Rhodamine 123	*r*-value	0.148	[a]**0.526**
Accumulation	*p*-value	0.0161	[a]**1.12×10^{-5}**
ABCB5 Expression			Maytansine
ABCB5 Expression	*r*-value	0.109	[a]**0.454**
(Microarray)	*p*-value	0.227	[a]**6.67×10^{-4}**
ABCB5 Expression	*r*-value	0.020	[a]**0.402**
(RT-PCR)	*p*-value	0.444	[a]**0.0026**
ABCC1 Expression			Vinblastine
DNA Gene	*r*-value	−0.089	[a]**0.429**
Copy Number	*p*-value	0.271	[a]**0.001**
ABCC1 Expression	*r*-value	0.193	[a]**0.398**
(Microarray)	*p*-value	0.092	[a]**0.003**
ABCC1 Expression	*r*-value	−0.0214	0.299
(RT-PCR)	*p*-value	0.449	[a]**0.036**
ABCG2 Expression			Pancratistatin
ABCG2 Expression	*r*-value	0.111	[a]**0.323**
(Microarray)	*p*-value	0.225	[a]**0.006**
ABCG2 Expression	*r*-value	0.129	[a]**0.346**
(Western Blot)	*p*-value	0.190	[a]**0.004**
EGFR Expression			Erlotinib
EGFR Expression	*r*-value	−0.167	[a]**-0.458**
(Microarray)	*p*-value	0.126	[a]**1.15×10^{-4}**
EGFR Expression	*r*-value	−0.105	[a]**-0.379**
(PCR Slot Blot)	*p*-value	0.235	[a]**0.002**
EGFR Expression	*r*-value	−0.122	[a]**-0.376**
(Protein Array)	*p*-value	0.201	[a]**0.002**
***TP53* Mutation**			5-Fluorouracil
TP53 Mutation	*r*-value	−0.214	[a]**-0.502**
(cDNA Sequencing)	*p*-value	0.072	[a]**3.50×10^{-5}**
TP53 Function	*r*-value	−0.073	[a]**-0.436**
(Yeast Functional Assay)	*p*-value	0.318	[a]**5.49×10^{-4}**
***NRAS* Mutation**			Doxorubicin
Codon 12 mutation	*r*-value	[a]**-0.652**	[a]**-0.424**
	p-value	[a]**6.11×10^{-7}**	[a]**9.61×10^{-4}**
HSP90			Geldanamycin
HSP90 Expression	*r*-value	0.248	[a]**-0.392**
(Microarray)	*p*-value	0.043	[a]**0.001**
GSTP1			Doxorubicin
GSTP1 Expression	*r*-value	−0.005	[a]**0.327**
(microarray)	*p*-value	0.486	[a]**0.005**
GSTP1 Expression	*r*-value	0.194	[a]**0.358**
(Northern blot)	*p*-value	0.091	[a]**0.002**
Proliferation			5-Fluorouracil
Cell Doubling Time	*r*-value	0.177	[a]**0.627**
	p-value	0.117	[a]**7–14×10^{-6}**

[a] $p < 0.05$ and $r > 0.3$ (or $r < -0.3$).

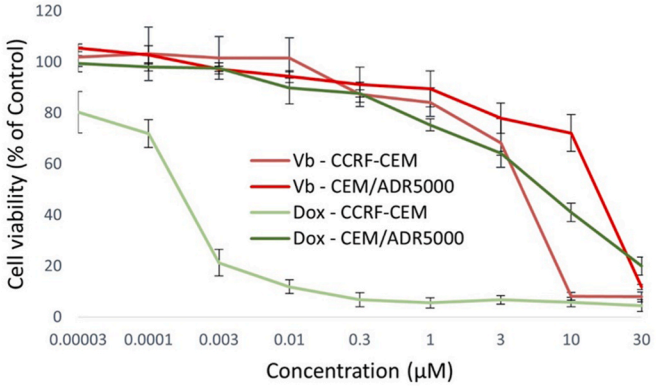

Fig. 8. Dose response curves of verbascoside and doxorubicin (control drug) of drug sensitive CCRF-CEM and multidrug-resistant P-glycoprotein (ABCB1)-overexpressing CEM/ADR5000 cells (Vb: Verbascoside, Dox: Doxorubicin) (mean ± SD of three independent experiments with each 6 parallel measurments).

comparative binding study of these two compounds to NLRP3 and NF-κB proteins. *In vitro* antioxidant activities (scavenging activity of DPPH and superoxide, xanthine oxidase inhibition) of both isomers were similar, while verbascoside showed higher inhibitory activity for AAPH-induced hemolysis and acetylcholinesterase than its isomer (Chen et al., 2012). In rats, orally administered verbascoside lowered systolic and diastolic blood pressure more than isoverbascoside, indicating superior antihypertensive activity.

Inflammation is often associated with the development and progression of cancer. Therefore, targeting inflammation represents an attractive strategy both for cancer prevention and for cancer therapy (Singh et al., 2019; Grivennikov et al., 2010; Zhiyu et al., 2016; Afonina et al., 2017; Khandia and Munjal, 2020). Most precancerous and cancerous tissues show signs of inflammation. This involves the movement of innate immune cells into the tissue, the presence of specific inflammatory signaling molecules (called cytokines and chemokines), changes in tissue structure (remodeling), and the formation of new blood vessels (angiogenesis). Cancer-associated inflammation promotes tumor growth and progression. For instance, innate immune cells called tumor-associated macrophages work their way into precancerous tissue and can then release factors promoting tumor growth and metastasis. Accordingly, in many human tumors, the infiltration of large numbers of these macrophages is associated with a poor survival prognosis. Moreover, increased expression of genes associated with macrophage infiltration (such as CD68) forms part of the molecular profile that heralds a poor prognosis in certain cancers (Mantovani, 2005). The inflammasome signal plays a direct role in the anti-tumor effects of chemotherapy agents by inducing pyroptosis and an indirect role by activating immune cells (Zhang et al., 2023). Chemotherapy induced NLRP3 activation leads to resistance to chemotherapeutic agents (Tengesdal et al., 2023). NLRP3 activation promoted 5-fluorouracil resistance of oral squamous cell carcinoma both *in vitro* and *in vivo* (Feng et al., 2017). The authors concluded that targeting the ROS/NLRP3 inflammasome/IL-1β signaling pathway could potentially enhance 5-FU-based adjuvant chemotherapy for OSCC. Chemotherapy-triggered NLRP3 activation was also seen in acute lymphoblastic lymphoma. Blocking NLRP3 activation inhibited the *in vitro* growth of ALL cells, induced apoptosis in both steroid-sensitive and steroid-resistant leukemia cells, and significantly prolonged the survival of mice bearing human PDX lines (Hu et al., 2020). In another study, NLRP3 activation was overexpressed in cisplatin-resistant ovarian cancer cells. Knockdown of the inflammasome inhibited the malignant progression of the resistant cells and offered a potential target for cisplatin-based ovarian cancer chemotherapy (Li et al., 2023). NF-κB also plays a crucial role in promoting cancer resistance to chemotherapy. NF-κB augmented the expression of the multidrug resistance (*MDR1*) gene in cancer cells (Bentires-Alj et al., 2003). Inhibition of NF-kB activity sensitized the resistant breast cancer cells to doxorubicin. Furthermore, cell migration was significantly suppressed in cells co-treated with both doxorubicin and NF-kB

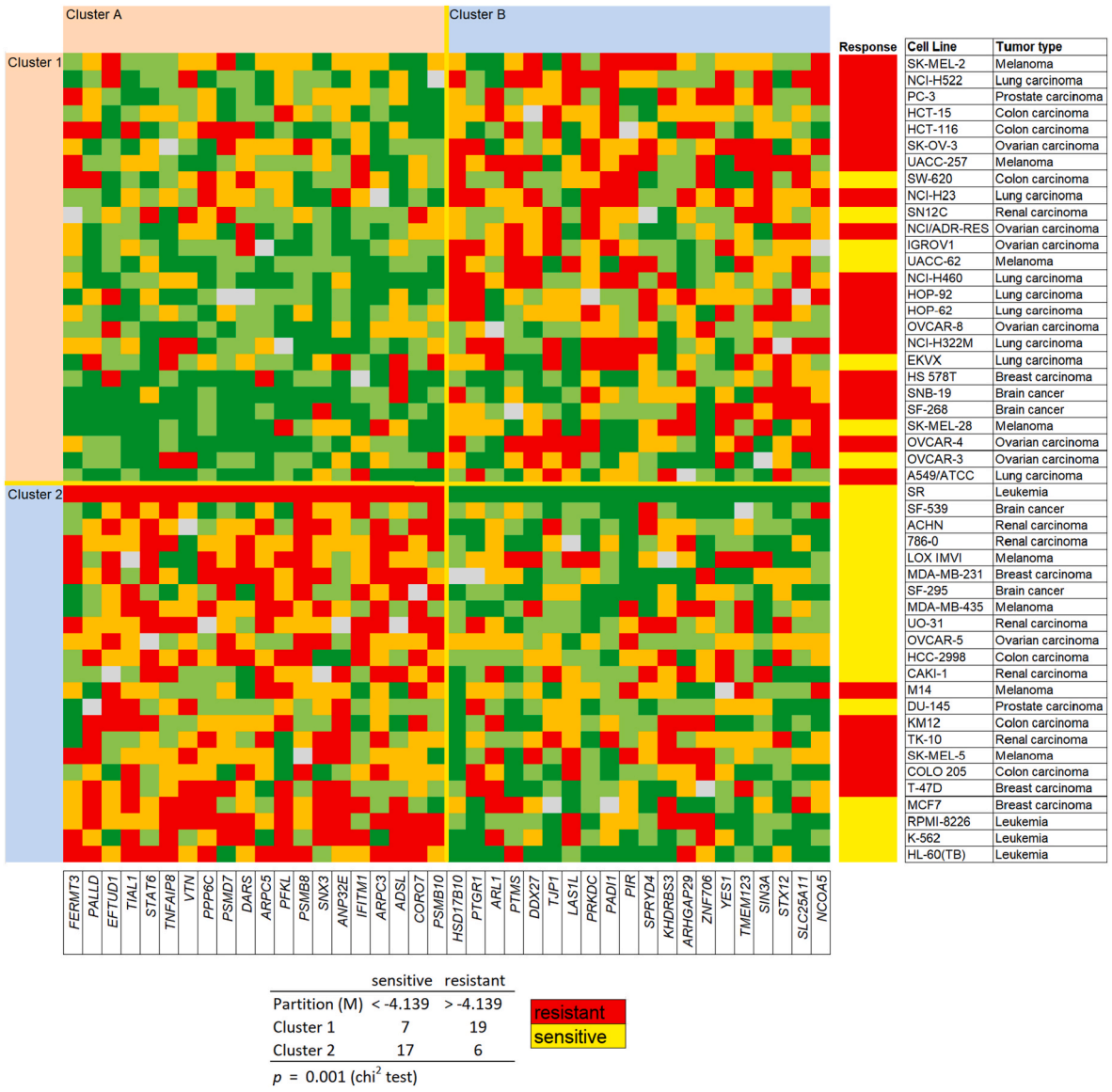

Fig. 9. Hierarchical cluster analysis (Ward method) of tumor proteomics (3171 proteins) in 49 tumor cell lines. The protein expressions have been labeled in different colors: red (high upregulation), orange (low upregulation), grey (median value), light green (low doenregulation), and dark green (high downregulation). The response of the cell lines to verbascoside has been defined as sensitive if the $\log_{10}IC_{50}$ value of the individual cell line was lower than the median value of all cell lines and defined as resistant if it was higher. (For interpretation of the references to color in this figure legend, the reader is referred to the Web version of this article.)

inhibitors (Abdin et al., 2021).

Therefore, we were interested in whether the NF-kB and NLRP3 inhibitors we identified, also exert cytotoxic activity toward cancer cells. Among the promising candidates were apigenin-derived natural products and verbascoside. Since we recently reported on the anticancer activity of apigenin and its molecular modes of action (Adham et al., 2021), we focused on verbascoside in the present investigation. Verbascoside (synonym: acetoside) was indeed cytotoxic towards a panel of 49 tumor cell lines of the NCI with the best cytotoxicity towards leukemia cells. A comparison with 81 standard anticancer agents revealed similarities to DNA-damaging agents, implying that verbascoside might also affect the integrity of tumor DNA.

Drug resistance and especially multidrug resistance jeopardizes the treatment success of many established anticancer drugs. It was therefore pleasing that the cytotoxicity of verbascoside did not correlate with most of the common drug resistance mechanisms, indicating that verbascoside may inhibit resistant tumor cells with similar efficacy to sensitive ones. This is an interesting finding since strategies to manage drug resistance in the clinic are urgently needed to improve treatment outcomes of chemotherapy and to prolong the survival times of patients. However, our analysis revealed a significant relationship between NRAS mutations and the response of tumor cells to verbascoside. The RAS oncogenes are long known as resistance mechanisms to DNA-damaging agents (Sklar, 1988; Kaufmann et al., 1995; Healy et al., 2022) and may also be operative in the case of verbascoside.

The fact that verbascoside was not involved in most of the common resistance mechanisms does not mean that there are no existing factors causing resistance to verbascoside. Therefore, we studied the proteomic expression profile of 3171 proteins in 49 NCI cell lines (Guo et al., 2015). It is well-known that the responsiveness to treatment of tumor cells is not only determined by resistance mechanisms but also by sensitivity factors (D'Andrea, 2018; Álvarez-Fernández and Malumbres, 2020; Lee et al., 2020). A prominent example is the anthracycline doxorubicin, and other drugs whose resistance is caused by high expression of the drug efflux transporter P-glycoprotein (ABCB1), but whose sensitivity is also influenced by high expression of DNA topoisomerase II (Schneider et al.,

1994; Liu et al., 2022). Therefore, we selected the top 20 proteins whose high expression correlated with resistance to verbascoside and the top 20 proteins whose high expression correlated with verbascoside sensitivity. The causal contribution of these 40 proteins for sensitivity or resistance is not yet known but warrants further investigation in the future.

In addition to apigenin glycosides and their derivatives, as well as verbascoside, our virtual drug screening approach for NF-κB and NLRP3 inhibitors also identified other natural products from the *Sideritis* genus, *e.g.,* forsythoside A. This compound was reported to inhibit the growth of metastasizing B16-F10 melanoma cells (Bao et al., 2017) in addition to its anti-inflammatory activity (Gong et al., 2021). Another compound in the phytochemical *Sideritis* library was martynoside. This compound exerted activity in 5-fluorouracil-induced bone marrow cytotoxicity *ex vivo* and *in vivo* without compromising the antitumor effect of 5-fluorouracil (Hong et al., 2021). Echinacoside, also a component of the library, was shown to inhibit colorectal cancer metastasis by regulating the gut microbiota and suppressing the PI3K/AKT signaling pathway (Wei et al., 2024). Ozturkosides act in an anti-inflammatory manner without significant anticancer effect (Küpeli et al., 2007). Some bioactivities for lavandulifolioside have been shown, but cytotoxic activities against cancer cells have not been reported so far. The anticancer activity of apigenin is well documented not only *in vitro* but also *in vivo* (Singh et al., 2022). The anticancer effect of verbascoside has been reported (Khan et al., 2022) but the presumable DNA-damaging effects reported here are new. Verbascoside has been reported to both prevent DNA damage induced by other agents and also to enhance the anticancer potential of other agents (Saxena et al., 2010; Peerzada et al., 2016). This contrasting data might be concentration-dependent and agent-specific and requires further investigation in the future.

5. Conclusions

In this study, we generated a phytochemical library containing 657 *Sideritis* compounds, which served for the virtual screening of NF-κB and NLRP3 inhibitors, indicating the anti-inflammatory potential of the top identified compounds. These top compounds included verbascoside, which is one of the most abundant compounds within the genus *Sideritis,* and also apigenin 7-,4′-bis(trans-*p*-coumarate). To the best of our knowledge, we report on the bioactivity of the latter compound for the first time in this study. The binding has been verified *in vitro* by microscale thermophoresis. As inflammation can trigger carcinogenesis, these compounds also exert cytotoxicity towards cancer cells. In the present study, we selected verbascoside and found that verbascoside inhibited cancer cells by using the NCI tumor cell line panel. Verbascoside may bypass resistance to standard cancer drugs established in the clinic and kill otherwise drug-resistant cells with similar efficacy as sensitive ones. Thus, verbascoside represents an interesting candidate compound that deserves further studies in the future.

CRediT authorship contribution statement

Rümeysa Yücer: Writing – original draft, Investigation, Formal analysis, Data curation. **Angela Schröder:** Writing – review & editing, Funding acquisition. **Gülaçtı Topçu:** Writing – review & editing, Funding acquisition, Data curation. **Thomas Efferth:** Writing – review & editing, Data curation, Conceptualization.

Declaration of competing interest

As corresponding author, I declare on behalf of all authors that there is no conflict of interest.

Acknowledgments

We are grateful for the foundations of the Scientific and Technological Research Council of Türkiye (TUBITAK) and the Theophrastus Paracelsus Foundation (Mühltal, Germany), as well as the partial support from Bezmialem Vakif University (BAP-12.2017/45) We extend our sincere thanks to Prof. Dr. Yuksel Kan for the botanical identification and Lara Friedrich for her invaluable time and effort in reading and reviewing the paper.

Appendix A. Supplementary data

Supplementary data to this article can be found online at https://doi.org/10.1016/j.jep.2024.119074.

Data availability

Data will be made available on request.

References

Abdin, S.M., Tolba, M.F., Zaher, D.M., Omar, H.A., 2021. Nuclear factor-κB signaling inhibitors revert multidrug-resistance in breast cancer cells. Chem. Biol. Interact. 340, 109450.
Aboutabl, E., Nassar, M., Elsakhawy, F., Maklad, Y., Osman, A., El-Khrisy, E., 2002. Phytochemical and pharmacological studies on *Sideritis taurica* Stephan ex Wild. J. Ethnopharmacol. 82, 177–184.
Adham, A.N., Abdelfatah, S., Naqishbandi, A.M., Mahmoud, N., Efferth, T., 2021. Cytotoxicity of apigenin toward multiple myeloma cell lines and suppression of iNOS and COX-2 expression in STAT1-transfected HEK293 cells. Phytomedicine 80, 153371.
Afonina, I.S., Zhong, Z., Karin, M., Beyaert, R., 2017. Limiting inflammation—the negative regulation of NF-κB and the NLRP3 inflammasome. Nat. Immunol. 18, 861–869.
Akcos, Y., Ezer, N., Calis, I., Demirdamar, R., Tel, B., 1999. Polyphenolic compounds of *Sideritis lycia* and their anti-inflammatory activity. Pharm. Biol. 37, 118–122.
Alcaraz, M.J., Tordera, M., 1988. Studies on the gastric anti-ulcer activity of hypolaetin-8-glucoside. Phytother Res. 2, 85–88.
Alipieva, K., Korkina, L., Orhan, I.E., Georgiev, M.I., 2014. Verbascoside–a review of its occurrence, (bio)synthesis and pharmacological significance. Biotechnol. Adv. 32, 1065–1076.
Alley, M.C., Scudiero, D.A., Monks, A., Hursey, M.L., Czerwinski, M.J., Fine, D.L., Abbott, B.J., Mayo, J.G., Shoemaker, R.H., Boyd, M.R., 1988. Feasibility of drug screening with panels of human tumor cell lines using a microculture tetrazolium assay. Cancer Res. 48, 589–601.
Álvarez-Fernández, M., Malumbres, M., 2020. Mechanisms of sensitivity and resistance to CDK4/6 inhibition. Cancer Cell 37, 514–529.
Aneva, I., Zhelev, P., Kozuharova, E., Danova, K., Nabavi, S.F., Behzad, S., 2019. Genus *Sideritis*, section Empedoclia in southeastern Europe and Turkey–studies in ethnopharmacology and recent progress of biological activities. DARU J. Pharm. Sci. 27, 407–421.
Armata, M., Gabrieli, C., Termentzi, A., Zervou, M., Kokkalou, E., 2008. Constituents of *Sideritis syriaca* ssp. *syriaca* (Lamiaceae) and their antioxidant activity. Food Chem. 111, 179–186.
Baldrighi, M., Mallat, Z., Li, X., 2017. NLRP3 inflammasome pathways in atherosclerosis. Atherosclerosis 267, 127–138.
Bao, J., Ding, R.B., Liang, Y., Liu, F., Wang, K., Jia, X., Zhang, C., Chen, M., Li, P., Su, H., et al., 2017. Differences in chemical component and anticancer activity of green and ripe Forsythiae Fructus. Am. J. Chin. Med. 45, 1513–1536.
Baytop, T., 1999. *Türkiye'de bitkiler ile tedavi: geçmişte ve bugün*; [Treatment with plants in Turkey: past and present]. Nobel Tıp Kitabevleri, Istanbul, p. 422 (in Turkish).
Bentires-Alj, M., Barbu, V., Fillet, M., Chariot, A., Relic, B., Jacobs, N., Gielen, J., Merville, M.-P., Bours, V., 2003. NF-κB transcription factor induces drug resistance through MDR1 expression in cancer cells. Oncogene 22, 90–97.
Bingol, Z., Kızıltaş, H., Gören, A.C., Kose, L.P., Topal, M., Durmaz, L., Alwasel, S.H., Gulcin, İ., 2021. Antidiabetic, anticholinergic and antioxidant activities of aerial parts of shaggy bindweed (*Convulvulus betonicifolia* Miller subsp.) – profiling of phenolic compounds by LC-HRMS. Heliyon 7, e06986.
Boaru, S.G., Borkham-Kamphorst, E., Van de Leur, E., Lehnen, E., Liedtke, C., Weiskirchen, R., 2015. NLRP3 inflammasome expression is driven by NF-κB in cultured hepatocytes. Biochem. Biophys. Res. Commun. 458, 700–706.
Bracey, N.A., Beck, P.L., Muruve, D.A., Hirota, S.A., Guo, J., Jabagi, H., Wright Jr., J.R., Macdonald, J.A., Lees-Miller, J.P., Roach, D., et al., 2013. The Nlrp3 inflammasome promotes myocardial dysfunction in structural cardiomyopathy through interleukin-1β. Exp. Physiol. 98, 462–472.
Bruno, M., Rosselli, S., Pibiri, I., Kilgore, N., Lee, K.-H., 2002. Anti-HIV agents derived from the e nt-kaurane diterpenoid linearol. J. Nat. Prod. 65, 1594–1597.
Çarıkçı, S., Kılıç, T., Gören, A.C., Dirmenci, T., Alim Toraman, G., Topçu, G., 2023. Chemical profile of the Anatolian *Sideritis* species with bioactivity studies. Pharm. Biol. 61, 1484–1511.
Cavalcanti, M.R.M., Passos, F.R.S., Monteiro, B.S., Gandhi, S.R., Heimfarth, L., Lima, B. S., Nascimento, Y.M., Duarte, M.C., Araujo, A.A.S., Menezes, I.R.A., et al., 2021. HPLC-DAD-UV analysis, anti-inflammatory and anti-neuropathic effects of

methanolic extract of *Sideritis bilgeriana* (Lamiaceae) by NF-kappa B, TNF-alpha, IL-1 beta and IL-6 involvement. J. Ethnopharmacol. 265, 113338.
Chen, C.-H., Lin, Y.-S., Chien, M.-Y., Hou, W.-C., Hu, M.-L., 2012. Antioxidant and antihypertensive activities of acteoside and its analogs. Bot. Stud. 53, 421–429.
Cheng, J., Liao, Y., Dong, Y., Hu, H., Yang, N., Kong, X., Li, S., Li, X., Guo, J., Qin, L., 2020. Microglial autophagy defect causes Parkinson disease-like symptoms by accelerating inflammasome activation in mice. Autophagy 16, 2193–2205.
Chittasupho, C., Srisawad, K., Arjsri, P., Phongpradist, R., Tingya, W., Ampasavate, C., Dejkriengkraikul, P., 2023. Targeting spike glycoprotein S1 mediated by NLRP3 inflammasome machinery and the cytokine releases in A549 lung epithelial cells by nanocurcumin. Pharmaceuticals 16, 862.
Coll, R.C., Hill, J.R., Day, C.J., Zamoshnikova, A., Boucher, D., Massey, N.L., Chitty, J.L., Fraser, J.A., Jennings, M.P., Robertson, A.A.B., et al., 2019. MCC950 directly targets the NLRP3 ATP-hydrolysis motif for inflammasome inhibition. Nat. Chem. Biol. 15, 556–559.
Cui, Y., Yu, H., Bu, Z., Wen, L., Yan, L., Feng, J., 2022. Focus on the role of the NLRP3 inflammasome in multiple sclerosis: pathogenesis, diagnosis, and therapeutics. Front. Mol. Neurosci. 15, 894298.
D'Andrea, A.D., 2018. Mechanisms of PARP inhibitor sensitivity and resistance. DNA Repair 71, 172–176.
De Las Heras, B., Navarro, A., Díaz-Guerra, M.J., Bermejo, P., Castrillo, A., Boscá, L., Villar, A., 1999. Inhibition of NOS-2 expression in macrophages through the inactivation of NF-κB by andalusol. Br. J. Pharmacol. 128, 605–612.
Dissook, S., Umsumarng, S., Mapoung, S., Semmarath, W., Arjsri, P., Srisawad, K., Dejkriengkraikul, P., 2023. Luteolin-rich fraction from *Perilla frutescens* seed meal inhibits spike glycoprotein S1 of SARS-CoV-2-induced NLRP3 inflammasome lung cell inflammation via regulation of JAK1/STAT3 pathway: a potential anti-inflammatory compound against inflammation-induced long-COVID. Front. Med. 9, 1072056.
Dulger, B., Ugurlu, E., Aki, C., Suerdem, T.B., Camdeviren, A., Tazeler, G., 2005. Evaluation of antimicrobial activity of some endemic *Verbascum, Sideritis*, and *Stachys* species from Turkey. Pharm. Biol. 43, 270–274.
Efferth, T., Konkimalla, V.B., Wang, Y.-F., Sauerbrey, A., Meinhardt, S., Zintl, F., Mattern, J., Volm, M., 2008. Prediction of broad spectrum resistance of tumors towards anticancer drugs. Clin. Cancer Res. 14, 2405–2412.
Ertas, A., Ozturk, M., Boga, M., Topcu, G., 2009. Antioxidant and anticholinesterase activity evaluation of ent-kaurane diterpenoids from *Sideritis arguta*. J. Nat. Prod. 72, 500–502.
Etemad, L., Zafari, R., Vahdati-Mashhadian, N., Moallem, S.A., Shirvan, Z.O., Hosseinzadeh, H., 2015. Acute, sub-acute and cell toxicity of verbascoside. Res. J. Med. Plant 9, 354–360.
Ezer, N., Sakar, M.K., Rodríguez, B., Torre, M.C.D., 1992. Flavonoid glycosides and a phenylpropanoid glycoside from *Sideritis perfoliata*. Int. J. Pharmacogn. 30, 61–65.
Farhat, A., Ben Hlima, H., Khemakhem, B., Ben Halima, Y., Michaud, P., Abdelkafi, S., Fendri, I., 2022. Apigenin analogues as SARS-CoV-2 main protease inhibitors: in silico screening approach. Bioengineered 13, 3350–3361.
Feng, X., Luo, Q., Zhang, H., Wang, H., Chen, W., Meng, G., Chen, F., 2017. The role of NLRP3 inflammasome in 5-fluorouracil resistance of oral squamous cell carcinoma. J. Exp. Clin. Cancer Res. 36, 81.
Flores, J., Noël, A., Fillion, M.-L., LeBlanc, A.C., 2022. Therapeutic potential of Nlrp1 inflammasome, Caspase-1, or Caspase-6 against Alzheimer disease cognitive impairment. Cell Death Differ. 29, 657–669.
Fraga, B.M., 2012. Phytochemistry and chemotaxonomy of *Sideritis* species from the Mediterranean region. Phytochemistry 76, 7–24.
Fraga, B.M., Hernández, M.G., Fernández, C., Santana, J.M., 2009. A chemotaxonomic study of nine Canarian *Sideritis* species. Phytochemistry 70, 1038–1048.
Fraga, B.M., Hernandez, M.G., Santana, J.M., Terrero, D., Galvan, M.F., 1995. A chemotaxonomical study of *Sideritis massoniana* taxa. Biochem. Systemat. Ecol. 23, 835–842.
Gong, L., Wang, C., Zhou, H., Ma, C., Zhang, Y., Peng, C., Li, Y., 2021. A review of pharmacological and pharmacokinetic properties of Forsythiaside A. Pharmacol. Res. 169, 105690.
Gonzalez, A.G., Fraga, B.M., Hernandez, M.G., Luis, J.G., Larruga, F., 1979. Comparative phytochemistry of the genus *sideritis* from the canary islands. Biochem. Systemat. Ecol. 7, 115–120.
González-Burgos, E., Carretero, M., Gómez-Serranillos, M., 2011. *Sideritis* spp.: uses, chemical composition and pharmacological activities - a review. J. Ethnopharmacol. 135, 209–225.
González-Burgos, E., Carretero, M.E., Gómez-Serranillos, M.P., 2013. Nrf2-dependent neuroprotective activity of diterpenoids isolated from *Sideritis* spp. J. Ethnopharmacol. 147, 645–652.
Gonzalez-Burgos, E., Duarte, A.I., Carretero, M.E., Moreira, P.I., Gomez-Serranillos, M.P., 2016. Kaurane diterpenes as mitochondrial alterations preventive agents under experimental oxidative stress conditions. Pharm. Biol. 54, 705–711.
Gora, I.M., Ciechanowska, A., Ladyzynski, P., 2021. NLRP3 inflammasome at the interface of inflammation, endothelial dysfunction, and type 2 diabetes. Cells 10, 314.
Goulas, V., Exarchou, V., Kanetis, L., Gerothanassis, I.P., 2014. Evaluation of the phytochemical content, antioxidant activity and antimicrobial properties of mountain tea (*Sideritis syriaca*) decoction. J. Funct.Foods 6, 248–258.
Govindarajan, V., de Rivero Vaccari, J.P., Keane, R.W., 2020. Role of inflammasomes in multiple sclerosis and their potential as therapeutic targets. J. Neuroinflammation 17, 260.
Grivennikov, S.I., Greten, F.R., Karin, M., 2010. Immunity, inflammation, and cancer. Cell 140, 883–899.
Gunbatan, T., Gurbuz, I., Bedir, E., Ozkan, A.M.G., Ozcinar, O., 2020. Investigations on the anti-ulcerogenic activity of *Sideritis caesarea* H. Duman, aytac & baser. J. Ethnopharmacol. 258, 112920.
Guo, T., Kouvonen, P., Koh, C.C., Gillet, L.C., Wolski, W.E., Röst, H.L., Rosenberger, G., Collins, B.C., Blum, L.C., Gillessen, S., 2015. Rapid mass spectrometric conversion of tissue biopsy samples into permanent quantitative digital proteome maps. Nat. Med. 21, 407–413.
Gürbüz, I., Özkan, A.M., Yesilada, E., Kutsal, O., 2005. Anti-ulcerogenic activity of some plants used in folk medicine of Pinarbasi (Kayseri, Turkey). J. Ethnopharmacol. 101, 313–318.
Güvenç, A., Okada, Y., Akkol, E.K., Duman, H., Okuyama, T., Çalış, İ., 2010. Investigations of anti-inflammatory, antinociceptive, antioxidant and aldose reductase inhibitory activities of phenolic compounds from *Sideritis brevibracteata*. Food Chem. 118, 686–692.
Halfon, B., Ciftci, E., Topcu, G., 2013. Flavonoid constituents of *Sideritis caesarea*. Turk. J. Chem. 37, 464–472. https://doi.org/10.3906/kim-1206-45.
Hanoğlu, D.Y., Hanoğlu, A., Yusufoğlu, H., Demirci, B., Başer, K.H.C., Çalış, İ., Yavuz, D.Ö., 2020. Phytochemical investigation of endemic *Sideritis cypria* post. Record Nat. Prod. 14, 105–115.
He, Y., Hara, H., Núñez, G., 2016. Mechanism and regulation of NLRP3 inflammasome activation. Trends Biochem. Sci. 41, 1012–1021.
Healy, F.M., Prior, I.A., MacEwan, D.J., 2022. The importance of Ras in drug resistance in cancer. Br. J. Pharmacol. 179, 2844–2867.
Heiner, F., Feistel, B., Wink, M., 2018. *Sideritis scardica* extracts inhibit aggregation and toxicity of amyloid-β in *Caenorhabditis elegans* used as a model for Alzheimer's disease. PeerJ 6, e4683.
Hernández-Pérez, M., Rabanal Gallego, R.M., 2002. Analgesic and antiinflammatory properties of *Sideritis lotsyi* var. *mascaensis*. Phytother Res. 16, 264–266.
Hong, M., Chen, D., Hong, Z., Tang, K., Yao, Y., Chen, L., Ye, T., Qian, J., Du, Y., Sun, R., 2021. Ex vivo and in vivo chemoprotective activity and potential mechanism of martynoside against 5-fluorouracil-induced bone marrow cytotoxicity. Biomed. Pharmacother. 138, 111501.
HPMC (Committee on Herbal Medicinal Products), 2015. Assessment report on *Sideritis scardica* Griseb.; *Sideritis clandestina* (Bory & Chaub.) Hayek; *Sideritis raeseri* Boiss. & Heldr.; *Sideritis syriaca* L., herba. European Union, Brussels, Belgium, p. 15. EMA/HMPC/39455/2015. https://www.ema.europa.eu/en/documents/herbal-report/final-assessment-report-sideritis-scardica-griseb-sideritis-clandestina-bory-chaub-hayek-sideritis-raeseri-boiss-heldr-sideritis-syriaca-l-herba_en.pdf. (Accessed 1 June 2024).
Hu, Z., Sporn, M., Letterio, J., 2020. Targeting NLRP3 inflammasome-induced therapy resistance in ALL. Blood 136, 46.
Islamuddin, M., Mustfa, S.A., Ullah, S., Omer, U., Kato, K., Parveen, S., 2022. Innate immune response and inflammasome activation during SARS-CoV-2 infection. Inflammation 245, 1849–1863.
Jeremic, I., Tadic, V., Isakovic, A., Trajkovic, V., Markovic, I., Redzic, Z., Isakovic, A., 2013. The mechanisms of in vitro cytotoxicity of mountain tea, *Sideritis scardica*, against the C6 glioma cell line. Planta Med. 79, 1516–1524.
Jüttler, E., Potrovita, I., Tarabin, V., Prinz, S., Dong-Si, T., Fink, G., Schwaninger, M., 2004. The cannabinoid dexanabinol is an inhibitor of the nuclear factor-kappa B (NF-κB). Neuropharmacology 47, 580–592.
Kaufmann, S.H., Kalemkerian, G.P., Jasti, R., Mabry, M., 1995. Effect of v-rasH on sensitivity of NCI-H82 human small cell lung cancer cells to cisplatin, etoposide, and camptothecin. Biochem. Pharmacol. 50, 1987–1993.
Khalid, S.A., Dawood, M., Boulos, J.C., Wasfi, M., Drif, A., Bahramimehr, F., Shahhamzehei, N., Shan, L., Efferth, T., 2022. Identification of gedunin from a phytochemical depository as a novel multidrug resistance-bypassing tubulin inhibitor of cancer cells. Molecules 27, 5858.
Khan, R.A., Hossain, R., Roy, P., Jain, D., Saikat, A.S.M., Shuvo, A.P.R., Akram, M., Elbossaty, W.F., Khan, I.N., Painuli, S., 2022. Anticancer effects of acteoside: mechanistic insights and therapeutic status. Eur. J. Pharmacol. 916, 174699.
Khandia, R., Munjal, A., 2020. Interplay between inflammation and cancer. Adv. Protein Chem. Struct. Biol. 119, 199–245.
Kilic, T., Topcu, G., Goren, A.C., Aydogmus, Z., Karagoz, A., Yildiz, Y.K., Aslan, I., 2020. Ent-kaurene diterpenoids from *Sideritis lycia* with antiviral and cytotoxic activities. Record Nat. Prod. 14, 256–268.
Kılıç, T., Yıldız, Y., Gören, A.C., Tümen, G., Topçu, G., 2003. Phytochemical analysis of some *Sideritis* species of Turkey. Chem. Nat. Compd. 39, 453–456.
Kimmig, A., Gekeler, V., Neumann, M., Frese, G., Handgretinger, R., Kardos, G., Diddens, H., Niethammer, D., 1990. Susceptibility of multidrug-resistant human leukemia cell lines to human interleukin 2-activated killer cells. Cancer Res. 50, 6793–6799.
Kinoshita, T., Imamura, R., Kushiyama, H., Suda, T., 2015. NLRP3 mediates NF-κB activation and cytokine induction in microbially induced and sterile inflammation. PLoS One 10, e0119179.
Kirmizibekmez, H., Ariburnu, E., Masullo, M., Festa, M., Capasso, A., Yesilada, E., Piacente, S., 2012. Iridoid, phenylethanoid and flavonoid glycosides from *Sideritis trojana*. Fitoterapia 83, 130–136.
Kırmızıbekmez, H., Erdoğan, M., Kúsz, N., Karaca, N., Erdem, U., Demirci, F., Hohmann, J., 2021. Secondary metabolites from the aerial parts of *Sideritis germanicopolitana* and their in vitro enzyme inhibitory activities. Nat. Prod. Res. 35, 655–658.
Kızıltaş, H., Bingol, Z., Gören, A.C., Kose, L.P., Durmaz, L., Topal, F., Alwasel, S.H., Gulcin, İ., 2021. LC-HRMS profiling and antidiabetic, anticholinergic, and antioxidant activities of aerial parts of kınkor (*Ferulago stellata*). Molecules 26, 2469.
Knörle, R., 2012. Extracts of *Sideritis scardica* as triple monoamine reuptake inhibitors. J. Neural. Transm. 119, 1477–1482.

Kucia, M., Ratajczak, J., Bujko, K., Adamiak, M., Ciechanowicz, A., Chumak, V., Brzezniakiewicz-Janus, K., Ratajczak, M.Z., 2021. An evidence that SARS-Cov-2/COVID-19 spike protein (SP) damages hematopoietic stem/progenitor cells in the mechanism of pyroptosis in Nlrp3 inflammasome-dependent manner. Leukemia 35, 3026–3029.

Küpeli, E., Şahin, F.P., Çalış, İ., Yeşilada, E., Ezer, N., 2007. Phenolic compounds of *Sideritis ozturkii* and their in vivo anti-inflammatory and antinociceptive activities. J. Ethnopharmacol. 112, 356–360.

Lee, S., Rauch, J., Kolch, W., 2020. Targeting MAPK signaling in cancer: mechanisms of drug resistance and sensitivity. Int. J. Mol. Sci. 21, 1102.

Li, W., Zhao, X., Zhang, R., Xie, J., Zhang, G., 2023. Silencing of NLRP3 sensitizes chemoresistant ovarian cancer cells to cisplatin. Mediat. Inflamm. 2023, 7700673.

Lin, X., Wang, H., An, X., Zhang, J., Kuang, J., Hou, J., Yan, M., 2021. Baeckein E suppressed NLRP3 inflammasome activation through inhibiting both the priming and assembly procedure: implications for gout therapy. Phytomedicine 84, 153521.

Liu, Z., Xing, L., Zhu, Y., Shi, P., Deng, G., 2022. Association between TOP2A, RRM1, HER2, ERCC1 expression and response to chemotherapy in patients with non-muscle invasive bladder cancer. Heliyon 8, e09643.

Loğoğlu, E., Arslan, S., Öktemer, A., Şaköyan, İ., 2006. Biological activities of some natural compounds from *Sideritis sipylea* Boiss. Phytother Res. 20, 294–297.

Menković, N., Goðevac, D., Milosavljević, S., Zdunić, G., Šavikin, K., Karadžić, I., 2010. Chemical composition and antimicrobial activity of *Sideritis raeseri* subsp. *raeseri* Hekdri. et Boiss. polar extracts. Planta Med. 76, LS6.

Mantovani, A., 2005. Inflammation by remote control. Nature 435, 752–753.

Moossavi, M., Parsamanesh, N., Bahrami, A., Atkin, S.L., Sahebkar, A., 2018. Role of the NLRP3 inflammasome in cancer. Mol. Cancer 17, 1–13.

Oosting, M., Buffen, K., van der Meer, J.W., Netea, M.G., Joosten, L.A., 2016. Innate immunity networks during infection with *Borrelia burgdorferi*. Crit. Rev. Microbiol. 42, 233–244.

Özer, Z., Gören, A.C., Kılıç, T., Öncü, M., Çarıkçı, S., Dirmenci, T., 2020. The phenolic contents, antioxidant and anticholinesterase activity of section Amaracus (Gled.) Vogel and Anatolicon Ietsw. of *Origanum* L. species. Arab. J. Chem. 13, 5027–5039.

Pan, P., Shen, M., Yu, Z., Ge, W., Chen, K., Tian, M., Xiao, F., Wang, Z., Wang, J., Jia, Y., et al., 2021. SARS-CoV-2 N protein promotes NLRP3 inflammasome activation to induce hyperinflammation. Nat. Commun. 12, 4664.

Peerzada, K.J., Faridi, A.H., Sharma, L., Bhardwaj, S.C., Satti, N.K., Shashi, B., Tasduq, S. A., 2016. Acteoside-mediates chemoprevention of experimental liver carcinogenesis through STAT-3 regulated oxidative stress and apoptosis. Environ. Toxicol. 31, 782–798.

Petreska, J., Stefova, M., Ferreres, F., Moreno, D., Tomás-Barberán, F., Stefkov, G., Kulevanova, S., Gil-Izquierdo, A., 2011. Potential bioactive phenolics of Macedonian *Sideritis* species used for medicinal "Mountain Tea". Food Chem. 125, 13–20.

Pike, A.F., Szabò, I., Veerhuis, R., Bubacco, L., 2022. The potential convergence of NLRP3 inflammasome, potassium, and dopamine mechanisms in Parkinson's disease. NPJ Parkinsons Dis 8, 1–9.

Piozzi, F., Bruno, M., Rosselli, S., Maggio, A., 2006. The diterpenoids from the genus *Sideritis*. In: Studies in Natural Products Chemistry, Atta Ur Raman, vol. 33. Elsevier, pp. 493–540.

Plioukas, M., Termentzi, A., Gabrieli, C., Zervou, M., Kefalas, P., Kokkalou, E., 2010. Novel acylflavones from *Sideritis syriaca* ssp. *syriaca*. Food Chem. 123, 1136–1141.

Qiu, H., Liu, W., Lan, T., Pan, W., Chen, X., Wu, H., Xu, D., 2018. Salvianolate reduces atrial fibrillation through suppressing atrial interstitial fibrosis by inhibiting TGF-β1/Smad2/3 and TXNIP/NLRP3 inflammasome signaling pathways in post-MI rats. Phytomedicine 51, 255–265.

Rodrigues, T.S., de Sá, K.S.G., Ishimoto, A.Y., Becerra, A., Oliveira, S., Almeida, L., Gonçalves, A.V., Perucello, D.B., Andrade, W.A., Castro, R., et al., 2021. Inflammasomes are activated in response to SARS-CoV-2 infection and are associated with COVID-19 severity in patients. J. Exp. Med. 218, e20201707.

Rodriguez-Linde, M., Diaz, R., Garcia-Granados, A., Quevedo-Sarmiento, J., Moreno, E., Onorato, M., Parra, A., Ramos-Cormenzana, A., 1994. Antimicrobial activity of natural and semisynthetic diterpenoids from *Sideritis* spp. Microbios 77, 7–13.

Saeed, M.E., Mahmoud, N., Sugimoto, Y., Efferth, T., Abdel-Aziz, H., 2018a. Betulinic acid exerts cytotoxic activity against multidrug-resistant tumor cells via targeting autocrine motility factor receptor (AMFR). Front. Pharmacol. 9, 481.

Saeed, M.E., Mahmoud, N., Sugimoto, Y., Efferth, T., Abdel-Aziz, H., 2018b. Molecular determinants of sensitivity or resistance of cancer cells toward sanguinarine. Front. Pharmacol. 9, 136.

Sarikurkcu, C., Locatelli, M., Mocan, A., Zengin, G., Kirkan, B., 2020. Phenolic profile and bioactivities of *Sideritis perfoliata* L.: the plant, its most active extract, and its broad biological properties. Front. Pharmacol. 10, 1642.

Saxena, A., Saxena, A., Singh, J., Bhushan, S., 2010. Natural antioxidants synergistically enhance the anticancer potential of AP9-cd, a novel lignan composition from *Cedrus deodara* in human leukemia HL-60 cells. Chem. Biol. Interact. 188, 580–590.

Schneider, E., Horton, J.K., Yang, C.-H., Nakagawa, M., Cowan, K.H., 1994. Multidrug resistance-associated protein gene overexpression and reduced drug sensitivity of topoisomerase II in a human breast carcinoma MCF7 cell line selected for etoposide resistance. Cancer Res. 54, 152–158.

Semmarath, W., Mapoung, S., Umsumarng, S., Arjsri, P., Srisawad, K., Thippraphan, P., Yodkeeree, S., Dejkriengkraikul, P., 2022. Cyanidin-3-*O*-glucoside and peonidin-3-*O*-glucoside-rich fraction of Black Rice germ and bran suppresses inflammatory responses from SARS-CoV-2 spike glycoprotein S1-induction in vitro in A549 lung cells and THP-1 macrophages via inhibition of the NLRP3 inflammasome pathway. Nutrients 14, 2738.

Sharma, B., Satija, G., Madan, A., Garg, M., Alam, M.M., Shaquiquzzaman, M., Khanna, S., Tiwari, P., Parvez, S., Iqubal, A., 2022. Role of NLRP3 inflammasome and its inhibitors as emerging therapeutic drug candidate for Alzheimer's disease: a review of mechanism of activation, regulation, and inhibition. Inflammation 46, 1–32.

Singh, N., Baby, D., Rajguru, J.P., Patil, P.B., Thakkannavar, S.S., Pujari, V.B., 2019. Inflammation and cancer. Ann. Afr. Med. 18, 121–126.

Singh, D., Gupta, M., Sarwat, M., Siddique, H.R., 2022. Apigenin in cancer prevention and therapy: a systematic review and meta-analysis of animal models. Crit. Rev. Oncol.-Hematol. 176, 103751.

Sklar, M.D., 1988. Increased resistance to cis-diamminedichloroplatinum (II) in NIH 3T3 cells transformed by ras oncogenes. Cancer Res. 48, 793–797.

Stanoeva, J.P., Stefova, M., Stefkov, G., Kulevanova, S., Alipieva, K., Bankova, V., Aneva, I., Evstatieva, L.N., 2015. Chemotaxonomic contribution to the *Sideritis* species dilemma on the Balkans. Biochem. Systemat. Ecol. 61, 477–487.

Suetomi, T., Willeford, A., Brand, C.S., Cho, Y., Ross, R.S., Miyamoto, S., Brown, J.H., 2018. Inflammation and NLRP3 inflammasome activation initiated in response to pressure overload by Ca^{2+}/calmodulin-dependent protein kinase II δ signaling in cardiomyocytes are essential for adverse cardiac remodeling. Circulation 138, 2530–2544.

Swanson, K.V., Deng, M., Ting, J.P.-Y., 2019. The NLRP3 inflammasome: molecular activation and regulation to therapeutics. Nat. Rev. Immunol. 19, 477–489.

Szekanecz, Z., Szamosi, S., Kovács, G.E., Kocsis, E., Benkő, S., 2019. The NLRP3 inflammasome - interleukin 1 pathway as a therapeutic target in gout. Arch. Biochem. Biophys. 670, 82–93.

Tadic, V.M., Jeremic, I., Dobric, S., Isakovic, A., Markovic, I., Trajkovic, V., Bojovic, D., Arsic, I., 2012. Anti-inflammatory, gastroprotective, and cytotoxic effects of *Sideritis scardica* extracts. Planta Med. 78, 415–427.

Tasheva, K., Georgieva, A., Denev, P., Dimitrova, L., Dimitrova, M., Misheva, S., Petkova-Kirova, P., Lazarova, M., Petrova, M., 2023. Antioxidant and antitumor potential of micropropagated Balkan endemic *Sideritis scardica* Griseb. Plants 12, 3924.

Tengesdal, I.W., Dinarello, C.A., Marchetti, C., 2023. NLRP3 and cancer: pathogenesis and therapeutic opportunities. Pharmacol. Ther. 251, 108545.

Toldo, S., Bussani, R., Nuzzi, V., Bonaventura, A., Mauro, A.G., Cannatà, A., Pillappa, R., Sinagra, G., Nana-Sinkam, P., Sime, P., Abbate, A., 2021. Inflammasome formation in the lungs of patients with fatal COVID-19. Inflamm. Res. 70, 7–10.

Topcu, G., Ertas, A., Ozturk, M., Dincel, D., Kilic, T., Halfon, B., 2011. Ent-kaurane diterpenoids isolated from *Sideritis congesta*. Phytochem. Lett. 4, 436–439.

Tunalier, Z., Kosar, M., Ozturk, N., Baser, K., Duman, H., Kirimer, N., 2004. Antioxidant properties and phenolic composition of *Sideritis* species. Chem. Nat. Compd. 40, 206–210.

van der Heijden, T., Kritikou, E., Venema, W., van Duijn, J., van Santbrink, P.J., Slütter, B., Foks, A.C., Bot, I., Kuiper, J., 2017. NLRP3 inflammasome inhibition by MCC950 reduces atherosclerotic lesion development in apolipoprotein E–deficient mice—brief report. Arterioscler. Thromb. Vasc. Biol. 37, 1457–1461.

Venditti, A., Bianco, A., Frezza, C., Serafini, M., Giacomello, G., Giuliani, C., Bramucci, M., Quassinti, L., Lupidi, G., Lucarini, D., 2016. Secondary metabolites, glandular trichomes and biological activity of *Sideritis montana* L. subsp. *Montana* from Central Italy. Chem. Biodivers. 13, 1380–1390.

Ververis, A., Ioannou, K., Kyriakou, S., Violaki, N., Panayiotidis, M.I., Plioukas, M., Christodoulou, K., 2023. *Sideritis scardica* extracts demonstrate neuroprotective activity against $A\beta_{25-35}$ toxicity. Plants 12, 1716.

Wei, J., Zheng, Z., Hou, X., Jia, F., Yuan, Y., Yuan, F., He, F., Hu, L., Zhao, L., 2024. Echinacoside inhibits colorectal cancer metastasis via modulating the gut microbiota and suppressing the PI3K/AKT signaling pathway. J. Ethnopharmacol. 318, 116866.

Xia, L., Tan, S., Zhou, Y., Lin, J., Wang, H., Oyang, L., Tian, Y., Liu, L., Su, M., Wang, H., Cao, D., Liao, Q., 2018. Role of the NFκB-signaling pathway in cancer. OncoTargets Ther. 11, 2063–2073. https://doi.org/10.2147/OTT.S161109.

Xiao, Y., Ren, Q., Wu, L., 2022. The pharmacokinetic property and pharmacological activity of acteoside: a review. Biomed. Pharmacother. 153, 113296.

Xu, H., Akinyemi, I.A., Chitre, S.A., Loeb, J.C., Lednicky, J.A., McIntosh, M.T., Bhaduri-McIntosh, S., 2022. SARS-CoV-2 viroporin encoded by ORF3a triggers the NLRP3 inflammatory pathway. Virology 568, 13–22.

Yalcinkaya, M., Liu, W., Islam, M.N., Kotini, A.G., Gusarova, G.A., Fidler, T.P., Papapetrou, E.P., Bhattacharya, J., Wang, N., Tall, A.R., 2021. Modulation of the NLRP3 inflammasome by sars-CoV-2 envelope protein. Sci. Rep. 11, 24432.

Yao, C., Veleva, T., Scott Jr, L., Cao, S., Li, L., Chen, G., Jeyabal, P., Pan, X., Alsina, K.M., Abu-Taha, I., 2018. Enhanced cardiomyocyte NLRP3 inflammasome signaling promotes atrial fibrillation. Circulation 138, 2227–2242.

Zhang, Z., Li, X., Wang, Y., Wei, Y., Wei, X., 2023. Involvement of inflammasomes in tumor microenvironment and tumor therapies. J. Hematol. Oncol. 16, 24.

Zhao, C., Zhao, W., 2020. NLRP3 Inflammasome - a key player in antiviral responses. Front. Immunol. 11, 211.

Zhiyu, W., Wang, N., Wang, Q., Peng, C., Zhang, J., Liu, P., Ou, A., Zhong, S., Cordero, M. D., Lin, Y., 2016. The inflammasome: an emerging therapeutic oncotarget for cancer prevention. Oncotarget 7, 50766.

Zhou, H., Zhang, C., Huang, C., 2021. Verbascoside attenuates acute inflammatory injury caused by an intracerebral hemorrhage through the suppression of NLRP3. Neurochem. Res. 46, 770–777.

Zhu, X., Sun, M., Guo, H., Lu, G., Gu, J., Zhang, L., Shi, L., Gao, J., Zhang, D., Wang, W., 2022. Verbascoside protects from LPS-induced septic cardiomyopathy via alleviating cardiac inflammation, oxidative stress and regulating mitochondrial dynamics. Ecotoxicol. Environ. Saf. 233, 113327.